

T. 6 Nº 3 **2025**

Vol. 6 No. 3 2025

ISSN 2687-153X (online) <u>physcomsys.ru</u> <u>https://www.doi.org/10.33910/2687-153X-2025-6-3</u> 2025. Vol. 6, no. 3

PHYSICS OF COMPLEX SYSTEMS

Mass Media Registration Certificate $\underline{El\ No.\ FS77-77889}$, issued by Roskomnadzor on 10 February 2020 Peer-reviewed journal Open Access Published since 2020 4 issues per year

Editorial Board

Editor-in-chief Alexander V. Kolobov (St Petersburg, Russia) Deputy Editor-in-chief Andrey K. Belyaev (St Petersburg, Russia) Deputy Editor-in-chief Dmitry E. Temnov (St Petersburg, Russia) Executive editor Alexey A. Kononov (St Petersburg, Russia) Alexander P. Baraban (Saint Petersburg, Russia) Sergey P. Gavrilov (Saint Petersburg, Russia) Vladimir M. Grabov (Saint Petersburg, Russia) Alexander Z. Devadriani (Saint Petersburg, Russia) Castro Arata Rene Alejandro (Saint Petersburg, Russia) Sergey A. Nemov (Saint Petersburg, Russia) Roman G. Polozkov (Saint Petersburg, Russia) Oleg Yu. Prikhodko (Almaty, Kazakhstan) Igor P. Pronin (St Petersburg, Russia) Alexey E. Romanov (St Petersburg, Russia) Pavel P. Seregin (St Petersburg, Russia) Feng Rao (Shenzhen, China) Yan Cheng (Shanghai, China)

Advisory Board

Gennady A. Bordovsky (St Petersburg, Russia) Aleksander V. Ivanchik (St Petersburg, Russia) Vladimir V. Laptev (St Petersburg, Russia) Alexander S. Sigov (Moscow, Russia)

Publishing house of Herzen State Pedagogical University of Russia 48 Moika Emb., Saint Petersburg 191186, Russia E-mail: <u>izdat@herzen.spb.ru</u> Phone: +7 (812) 312-17-41

> Data size 3,22 Mbyte Published at 27.10.2025

The contents of this journal may not be used in any way without a reference to the journal "Physics of Complex Systems" and the author(s) of the material in question.



Editor of the English text K. Yu. Rybachuk Corrector N. A. Sinenikolskaya Cover design by O. V. Rudneva Layout by D. V. Romanova

CONTENTS

Condensed Matter Physics	121
Komarov V. A., Grabov V. M., Prostova V. V. Effect of a transverse electric field on the resistance of Bi thin films on a mica and polyimide substrate	. 121
Pronin V. P., Krushelnitckii A. N., Staritsyn M. V., Senkevich S. V., Kaptelov E. Yu., Pronin I. P., Tomkovid V. A. Microstructure features of spherulitic lead zirconate titanate thin films	. 127
Physics of Semiconductors	134
Goryaev M. A., Smirnov A. P. Spectra and kinetics of dye-sensitized photovoltaic effect in silicon	. 134
$Marchenko\ A.\ V.,\ Petrushin\ Yu.\ A.,\ Seregin\ P.\ P.,\ Doronin\ V.\ A.\ Analysis\ of\ the\ local\ structure$ of the nearest environment of germanium atoms in chalcogenide alloys ${\rm Ge_2Sb_2Te_5}$ using the Mössbauer spectroscopy method	. 139
Nemov S. A., Andreeva V. D., Aliabev A. Yu. Composition, structure and properties of PbSb ₂ Te ₄ crystals grown by the Chokhralsky method	. 144
Theoretical physics	150
Yakovleva S. A., Vahrushev V. A., Stepanov I. G., Belyaev A. K. Pseudopotential method for coupling matrix elements calculations	. 150
Summaries in Russian	155



Condensed Matter Physics.
Solid state physics

UDC 538.935

EDN AJAUNX

https://www.doi.org/10.33910/2687-153X-2025-6-3-121-126

Effect of a transverse electric field on the resistance of Bi thin films on a mica and polyimide substrate

V. A. Komarov^{⊠1}, V. M. Grabov¹, V. V. Prostova¹

¹ Herzen State Pedagogical University of Russia, 48 Moika Emb., Saint Petersburg 191186, Russia

Authors

Vladimir A. Komarov, ORCID: 0000-0002-2482-0885, e-mail: va-komar@yandex.ru

Vladimir M. Grabov, ORCID: 0000-0003-0215-6474, e-mail: vmgrabov@yandex.ru

Veronika V. Prostova, ORCID: 0009-0008-5478-4767, e-mail: school.nika.prostova@gmail.com

For citation: Komarov, V. A., Grabov, V. M., Prostova, V. V. (2025) Effect of a transverse electric field on the resistance of Bi thin films on a mica and polyimide substrate. *Physics of Complex Systems*, 6 (3), 121–126. https://www.doi.org/10.33910/2687-153X-2025-6-3-121-126 EDN AJAUNX

Received 29 June 2025; reviewed 16 July 2025; accepted 18 July 2025.

Funding: the research was supported by an internal grant of Herzen State Pedagogical University of Russia (project No. 50-VG)

Copyright: © V. A. Komarov, V. M. Grabov, V. V. Prostova (2025). Published by Herzen State Pedagogical University of Russia. Open access under CC BY License 4.0.

Abstract. This work studies the effect of a transverse electric field on the resistance of bismuth thin films. The existence of an electric field effect in bismuth thin films on mica and polyimide has been experimentally confirmed. The study obtained experimental dependences of resistance on the transverse electric field strength for bismuth films of various thicknesses on mica and polyimide. It also revealed changes associated with a decrease in the thickness of the film and the material of the used substrate. A qualitative interpretation of the observed effect was given based on the analysis of changes in the mobility of free charge carriers in films depending on the direction of the electric field, as well as the thickness of the film and the substrate material.

Keywords: bismuth, thin films, resistance, transverse electric field effect

Introduction

The effect of the transverse electric field in semiconductors has been thoroughly studied. It is a powerful tool for changing the electronic properties of the near-surface layers of a semiconductor. This effect currently underlies the technology of the silicon microelectronics metal-dielectric semiconductor.

The use of the electric field effect (EFE) to change the electronic properties of semimetals, bismuth and its antimony alloys, is a matter of interest. EFE can lead to new effects given the peculiarities of the energy spectrum of charge carriers in semimetals.

EFE in semimetals has not been studied to date. There are several papers on the study of EFE in bismuth films (Butenko et al. 1997; 1999; 2000), but the information contained in them does not provide a holistic picture of how this effect manifests itself in semi-metals. All of the above factors prompted us to study EFE in films of semimetals. We have conducted a study of EFE in films of the bismuth-antimony system up to 12 at. % Sb on a mica substrate. The results were presented in (Grabov et al. 2023). A significant change in the field dependence of the resistance on the film composition was found. An increase in the antimony concentration leads to a change in the sign of the effect to the opposite. A significant dependence of the effect on the film thickness was found. We explained these changes by the changing mobility ratio of free charge carriers.

To confirm the proposed explanation of the EFE change, we conducted a study of the effect of crystal-lite sizes on EFE in films of semimetals.

Experiment

The research was carried out on films of pure bismuth. The films were obtained by vacuum thermal spraying in a vacuum of 10^{-5} Torr. Muscovite mica with a thickness of 20-40 microns and polyimide with a thickness of 30 microns were used as the substrate. The film was sprayed onto the substrate at a temperature of 120° C, followed by annealing at a temperature of 250° C. The annealing time was 30 min. (Grabov et al. 2023). Films with a thickness of 50-500 nm were studied. The film deposition modes used ensure the production of large-block films on a mica substrate (the block sizes are much larger than the film thickness). The crystallographic orientation of the film crystal is such that the plane (111) of the crystal is parallel to the plane of the film (Grabov et al. 2017). Bismuth films on polyimide have significantly smaller block sizes, and the (111) plane can have a misorientation of up to 10° relative to the substrate plane. The effect of the transverse electric field on film resistance was studied on a capacitor structure in which the substrate was a dielectric. A bismuth film was applied to one side of the substrate, and a metal field electrode was applied to the other (Fig. 1). The bismuth film had contact pads for passing current and measuring the voltage drop. The field electrode covered only the active part of the bismuth film. The geometric dimensions of the active part of the film were 1 mm in width and 0.5 mm in length.

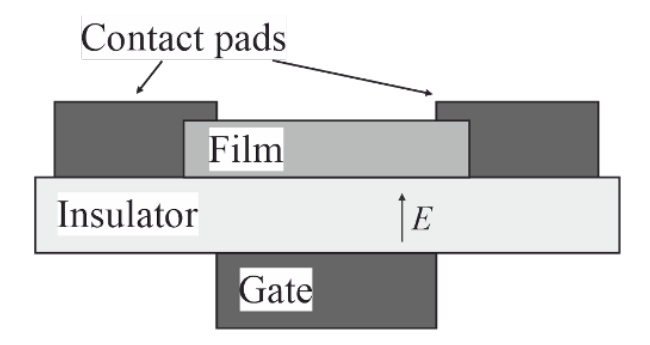


Fig. 1. Diagram of the samples under study

The measurements were carried out using direct current of the film and alternating voltage at the field electrode, which made it possible to directly measure the change in film resistance from the potential at the field electrode. This method improved the repeatability and accuracy of the results obtained. The measurements were carried out in the frequency range of 50–200 Hz. The polarity of the control field was determined by the polarity of the field electrode, i. e. a positive polarity meant that the film under study was negatively charged. The measurements were taken at temperatures of 77 K and 300 K.

Experimental results

The results of the study into the effect of the transverse electric field on the resistance of Bi films of various thicknesses on mica at 77 K are shown in Fig. 2.

As can be seen from the figure above, the dependence of the resistance on the transverse field changes significantly with the thickness of the film. In films of large thickness (500 nm, 250 nm), it has a nonlinear character, both with positive and negative polarity at the field electrode. In films of this composition, with a positive potential at the field electrode, a monotonous rise in film resistance is observed with increasing field strength. The relative magnitude of the change increases with decreasing film thickness. With a negative polarity at the field electrode, the resistance of films with a thickness of 50 nm and 100 nm goes down.

In films of higher thickness, resistance decreases first and then increases. The position of the minimum resistance of the film shifts to a region of greater negative field strength as film thickness decreases. For the 250 nm film, the minimum is thus reached at 75 MV/m, and for the 50 nm film, the minimum is just beginning, and there is no increase in resistance within the achievable control field strength.

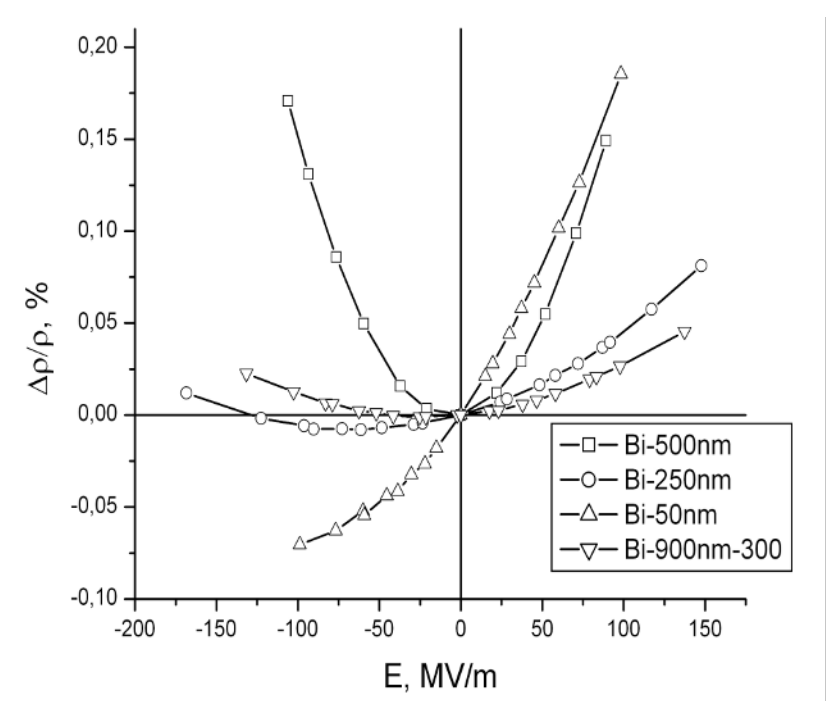


Fig. 2. Relative change in the resistance of Bi films of various thicknesses on mica depending on the electric field strength at $T=77~{\rm K}$

A rise in temperature leads to a decrease in the relative change in film resistance. For comparison, Fig. 2 also shows dependence for a 900 nm thick bismuth film at a temperature of 300 K. Although the magnitude of the change in resistance is less than at 77 K, the nature of dependence is similar to the dependence at 77 K.

Fig. 3 shows the study findings relating to the effect of EFE on the resistance of bismuth films on polyimide. The figure presents a significant change in the dependence of resistance on the strength of the transverse electric field. Films of all the studied thicknesses on polyimide have similar dependences with a minimum near the electric field strength equal to zero. However, it should be noted that the position of the minimum dependence varies with thickness. In the films with a thickness of 500 nm and 250 nm, it is located at negative values of the control field, and in the 50-nm film, in the region of a small positive field. For the film with a thickness of 100 nm, it practically coincides with a field strength of zero.

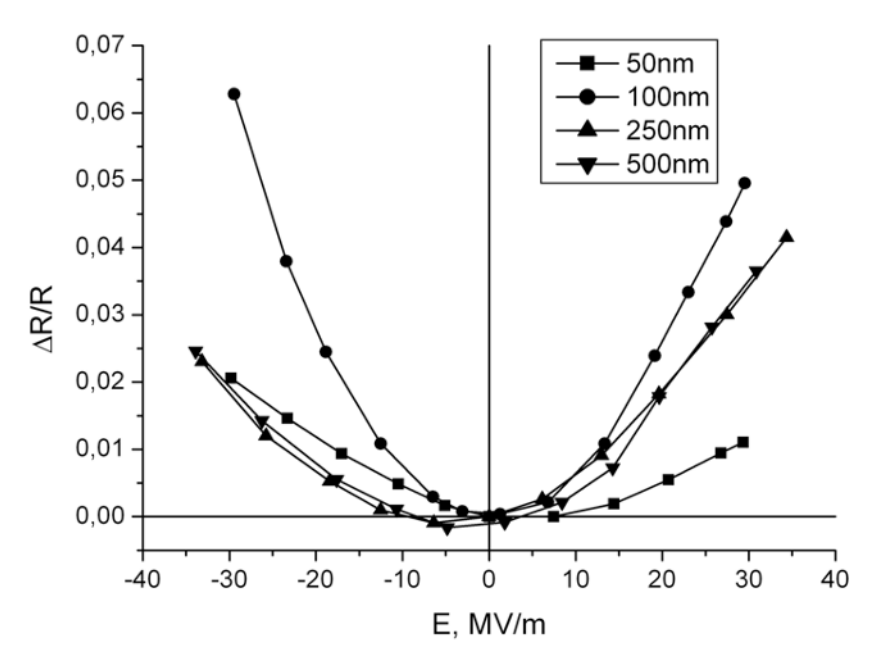


Fig. 3. Relative change in the resistance of Bi films of various thicknesses on polyimide depending on the electric field strength at T = 77 K

Our studies have shown that reducing the size of blocks in bismuth films significantly changes the effect of the transverse electric field on the resistance of the films.

Discussion

As we have already noted, the effect of the transverse electric field in semiconductors and semimetals is significantly different. In semiconductors, the concentration of intrinsic charge carriers is several orders of magnitude lower than in semimetals, and the conductivity is determined mainly by impurity charge carriers, while the mobility of charge carriers is weakly dependent on or independent of their concentration.

In semimetals, the concentration of intrinsic charge carriers is high, so in bismuth, even at 4.2 K, the concentration of free charge carriers is $3 \cdot 10^{23} \text{ I/m}^3$. The introduction of donor or acceptor impurities up to a certain point only changes the ratio between the concentrations of electrons and holes in the semimetal. In addition, an increase in the concentration of charge carriers is accompanied by a decrease in their mobility. This is clearly seen in the dependence of the resistivity of bismuth single crystals on the degree of doping with donor and acceptor impurities. Fig. 4, for example, shows the dependence of the resistivity of a single crystal of bismuth doped with tin on the degree of alloying.

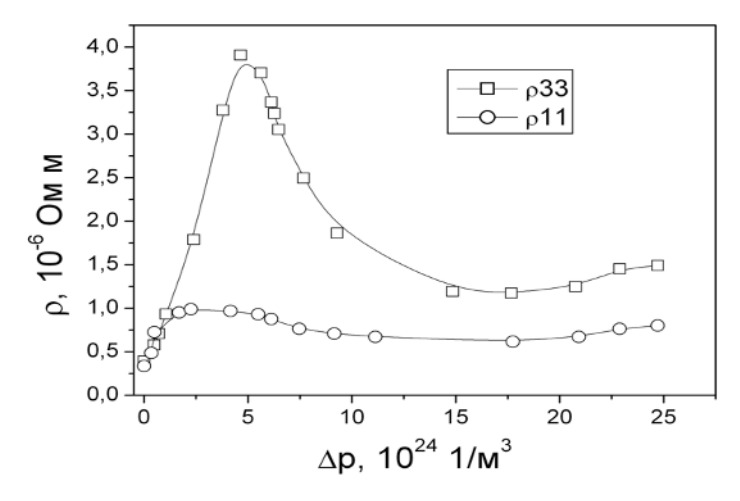


Fig. 4. Dependence of the resistivity of a single crystal of bismuth doped with tin on the difference in the concentrations of holes and electrons. T = 80 K

An increase in hole concentration during tin alloying leads to a rise in the resistivity of the bismuth single crystal. The effect of a transverse electric field on bismuth films is similar to the effect of doping these films with donor and acceptor impurities.

The second feature of the transverse electric field in semimetals is the small thickness of the shielding in these substances, which is a consequence of the high concentration of free charge carriers compared with semiconductors. In bismuth at 4.2 K, for example, calculation gives a screening thickness of about 9 nm. In semiconductors with weak doping, this value can reach tens of micrometers. However, given that the dependence is exponential, it can be assumed that the changing concentration in the 'tails' of the exponent changes film resistance.

The third factor contributing to the effect of the transverse electric field on the resistance of thin films of semimetals is the classical dimensional effect. The peculiarity of the anisotropy of the properties of charge carriers in bismuth and bismuth-antimony alloys leads to the fact that the dimensional effect on the film thickness and block sizes can change the ratio of the contributions of electrons and holes to kinetic effects. This can lead to a change in the manifestation of the effect in films of different thicknesses. This mechanism is reviewed in detail using the example of the Hall and Seebeck effects in (Komarov et al. 2019).

One should also take into account that the bismuth film on the substrate is strongly deformed. This deformation leads to a change in the concentration of free charge carriers. At 77 K, the concentration of free charge carriers in a bismuth film on mica is about 0.75 concentrations in a single crystal and 2.9 concentrations in a single crystal in a polyimide film. This also leads to an additional change in carrier mobility. This

is most evident in differential kinetic effects, such as the Hall effect. For example, Fig. 5 shows the temperature dependences of the Hall coefficient of bismuth films with a thickness of 800 nm with a different ratio of film thickness (L) and crystallite size (D).

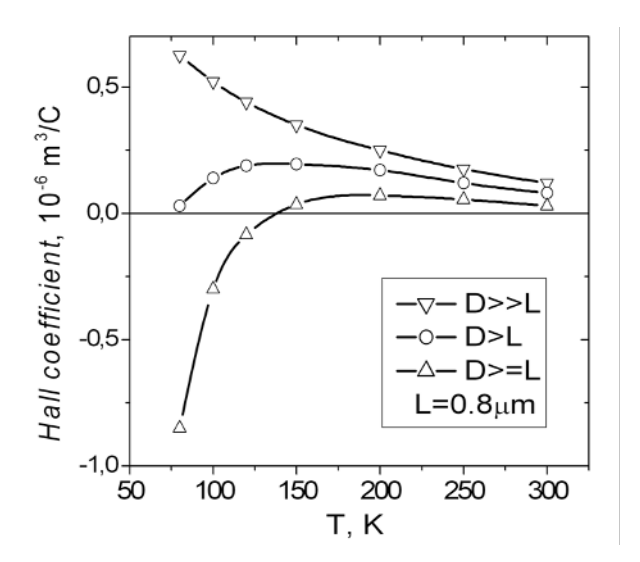


Fig. 5. Temperature dependence of the Hall coefficient of bismuth films with a thickness of 800 nm on mica with a different ratio of block size and film thickness

The above facts can elucidate the observed experimental dependencies. When a positive potential is applied to the field electrode, the film becomes negatively charged, which increases the concentration of electrons and reduces the concentration of holes. Considering that in a bismuth film with a large block size the mobility of holes is higher than that of electrons, such an elevated concentration of electrons leads to a higher resistance of the film. A change in the polarity on the control electrode induces the enrichment of the film with holes and a decrease in the number of electrons. At the initial stage, this leads to a reduced film resistance. With a rise in the excess concentration of the holes, the film resistance goes up due to a decrease in their mobility (Grabov et al. 2023)

Conclusion

Our study experimentally confirmed the existence of EFE in bismuth thin films. The dependence of the EFE value on the film thickness was obtained: as the film thickness decreases, the effect increases. A significant influence of the substrate material on the magnitude and nature of the EFE dependence was found, and a qualitative interpretation of the observed effect and its changes was given.

Due to the small magnitude of the effect, it can serve as an additional tool for the study of electronic and hole subsystems in bismuth thin films.

Conflict of Interest

The authors declare that there is no conflict of interest, either existing or potential.

Author Contributions

Vladimir Grabov — editing, supervision; Vladimir Komarov — research concept development, data analysis, editing, supervision; Veronika Prostova —producing samples, measurements of electrical properties. All the authors have read and agreed to the published version of the manuscript.

References

Butenko, A. V., Sandomirsky, V., Schlesinger, Y. et al. (1997) Characterization of the electrical properties of semimetallic Bi films by electrical field effect. *Journal of Applied Physics*, 82 (3), 1266–1273. http://dx.doi.org/10.1063/1.365897 (In English)

- Butenko, A. V., Shvarts, D., Sandomirsky, V. et al. (1999) The cause of the anomalously small electric field effect in thin films of Bi. *Applied Physics Letters*, 75 (11), 1628–1630. http://dx.doi.org/10.1063/1.124776 (In English)
- Butenko, A. V., Shvarts, D., Sandomirsky, V. et al. (2000) Hall constant in quantum-sized semimetal Bi films: Electric field effect influence. *Physica B: Condensed Matter*, 88 (5), 2634–2640. http://dx.doi.org/10.1063/1.1288166 (In English)
- Grabov, V. M., Komarov, V. A., Demidov, E. V. et al. (2017) Temperature dependences of galvanomagnetic coefficients of bismuth-antimony thin films 0–15 at.% Sb on substrates with different temperature expansion. *Humanities & Science University Journal*, 35, 48–57. (In English)
- Grabov, V. M., Komarov, V. A., Pozdnyakov, S. V. et al. (2023) Effect of a transverse electric field on the resistance of thin films of the Bi_{1-x} Sb_x (x = 0-0.12) system on mica. *Physics of Complex Systems*, 4 (2), 75–80 https://doi.org/10.33910/2687-153X-2023-4-2-75-80 (In English)
- Komarov, V. A., Grabov, V. M., Suslov, A. V. et al. (2019) The Hall end Seebeck Effects in bismuth thin films on mica substrates in temperature range of 77–300 K. *Semiconductors*, 53 (5), 593–598. https://doi.org/10.1134/51063782619050105 (In English)



Condensed Matter Physics.
Solid state physics

UDC 537.226.4 + 538.911

EDN ESOLRP

https://www.doi.org/10.33910/2687-153X-2025-6-3-127-133

Microstructure features of spherulitic lead zirconate titanate thin films

V. P. Pronin ^{⊠1}, A. N. Krushelnitckii ¹, M. V. Staritsyn ², S. V. Senkevich ^{1,3}, E. Yu. Kaptelov ³, I. P. Pronin ³, V. A. Tomkovid ¹

Herzen State Pedagogical University of Russia, 48 Moika Emb., Saint Petersburg 191186, Russia
 NRC "Kurchatov Institute" — CRISM "Prometey", 49 Shpalernaya Str., Saint Petersburg 191015, Russia
 Ioffe Institute, 26 Politekhnicheskaya Str., Saint Petersburg 194021, Russia

Authors

Vladimir P. Pronin, ORCID: 0000-0003-0997-1113, e-mail: pronin.v.p@yandex.ru

Artemii N. Krushelnitckii, ORCID: 0000-0003-3543-8531, e-mail: akrushelnitckii@herzen.spb.ru

Mikhail V. Staritsyn, ORCID: 0000-0002-0088-4577, e-mail: ms_145@mail.ru

Stanislav V. Senkevich, ORCID: 0000-0002-4503-1412, e-mail: senkevichsv@mail.ioffe.ru

Evgeny Yu. Kaptelov, ORCID: 0000-0002-7423-6943, e-mail: kaptelov@mail.ioffe.ru

Igor P. Pronin, ORCID: 0000-0003-3749-8706, e-mail: petrovich@mail.ioffe.ru

Vladislav A. Tomkovid, ORCID: 0009-0009-6601-2569, e-mail: vtomkovid@bk.ru

For citation: Pronin, V. P., Krushelnitckii, A. N., Staritsyn, M. V., Senkevich, S. V., Kaptelov, E. Yu., Pronin, I. P., Tomkovid, V. A. (2025) Microstructure features of spherulitic lead zirconate titanate thin films. *Physics of Complex Systems*, 6 (3), 127–133. https://www.doi.org/10.33910/2687-153X-2025-6-3-127-133 EDN ESOLRP

Received 24 June 2025; reviewed 16 July 2025; accepted 18 July 2025.

Funding: the study was supported by an internal grant of Herzen State Pedagogical University of Russia, No. 84 VN. *Copyright:* © V. P. Pronin, A. N. Krushelnitckii, M. V. Staritsyn, S. V. Senkevich, E. Yu. Kaptelov, I. P. Pronin, V. A. Tomkovid (2025). Published by Herzen State Pedagogical University of Russia. Open access under <u>CC BY License 4.0</u>.

Abstract. This study examines differences in the microstructure of spherulitic PZT films, in which low-angle non-crystalline and crystalline branching is realized during the perovskite phase crystallization, using scanning electron microscopy. It is assumed that the circular-step and radial boundaries observed in the films are formed due to the disclination mechanism, while their absence is the result of the sequential formation of single edge dislocations.

Keywords: spherulites, thin PZT films, mechanical stresses, mechanisms of crystal lattice tilting

Introduction

Research into the crystallization processes of thin polycrystalline films of lead zirconate titanate (Pb(Zr,Ti)O₃ or PZT) showed that the perovskite phase takes the form of nucleation and growth of individual islands (spherulites) with their subsequent merging and formation of a block structure. The images obtained by scanning electron microscopy (SEM) and the optical method revealed three types of islands observed, characterized by a) a concentric microstructure (Kwok, Desu 1994; Pronin 2017; Pronin et al. 1997) b) a radial-radiant microstructure (Carim et al. 1991; Preston, Haertling 1992; Spierings et al. 1993), and c) a microstructure with orientational correlation of crystalline grains in the plane of the film, distinguished by patterns of intersecting lines and nodes resulting from electron channeling (Alkoy et al. 2007; Staritsyn et al. 2024).

Direct optical observations of the circular structure crystallization of perovskite islands revealed its nonlinear nature in time: rapid growth of the islands was replaced by slow or 'shelf' growth, which was

then again replaced by rapid growth (Pronin 2017). The second thing discovered was a two-stage process of perovskite phase crystallization. The growth of the spherulite, characterized by low density with a porous structure, was observed at the first stage, and a denser modification of the perovskite phase was formed as a result of recrystallization at the second (Krupanidhi 1992; Pronin et al. 2010).

Circular-step growth in the form of concentric boundaries of the dense perovskite phase appeared most clearly (Pronin et al. 2010). It was suggested that such circular boundaries are boundaries of disturbances in the crystal structure, and their appearance is apparently associated with a significant difference in the densities of the low-temperature pyrochlore and perovskite phases, which, according to X-ray structural analysis, was ≈ 8% (Pronin et al. 1997). This has as a consequence the emergence of strong lateral mechanical stresses acting on the perovskite island from the low-temperature pyrochlore matrix. Film thickness shrinkage, which can reach 3-5% of the film thickness (Staritsyn et al. 2023), leads to significant relaxation of mechanical stresses. Nevertheless, estimates of residual strain calculated from the lattice rotation of electron backscatter diffraction data show that the strain can reach \sim 0.75%, and the magnitude of tensile stresses is \sim 0.9 GPa (Pronin et al. 2024). Since the above-described circular-step, radial-radiant, and axially uniformly deformed microstructures are inherent in many spherulitic formations of organic and inorganic materials that differ in composition and crystal structure (Da et al. 2024; Lutjes et al. 2021; Musterman et al. 2022; Savytskii et al. 2016; Shtukenberg et al. 2012; Woo, Lugito 2016), questions arise about how these microstructures are combined with each other and what their growth mechanisms are. To address these issues, we studied such microstructures in thin-film PZT spherulites using scanning electron microscopy.

Objects and methods of research

The objects of the study were thin PZT films with a composition corresponding to the region of the morphotropic phase boundary with the elemental ratio Zr/Ti = 54/46. The films were deposited by RF magnetron deposition on 'cold' platinized silicon or sitall ST-50 substrates and then subjected to high-temperature annealing at 530–580 °C to obtain either island perovskite films or single-phase block films (Staritsyn et al. 2023; 2024). The microstructure of the films was studied by scanning electron microscopy (Lira3 Tescan and EVO-40 Zeiss). The phase state was determined by the method of X-ray phase analysis θ -2 θ (Rigaku Ultima IV) and by the optical method (Nikon Eclipse LV150).

Results and discussion

Fig. 1 shows SEM images of the spherulitic island of PZT films formed on a silicon substrate, obtained in different modes. The image in Fig. 1a was taken in the backscattered electron mode (BSE mode), which points to the presence of circular boundaries and, therefore, circular-step growth of islands. These boundaries are clearly visible with normal incidence of the probing beam and detection of backscattered electrons, which indicates a vertical arrangement relative to the plane of the film. The same island is presented in Fig. 1b as a GROD map (grain reference orientation deviation), which is an interpretation of electron backscatter diffraction data and reflects the distribution of misorientation angles in the island relative to the average orientation of the growth axis, which, as a rule, falls on the center of the spherulite. The presence of a radial-radiant structure suggests an axially non-uniform rotation of the growth axis (or crystal lattice) in the island. Thus, the use of various modes of electron scanning of PZT thin films revealed the structural dualism of the growth of spherulitic islands.

Fig. 2 shows a change in the rotation angle of the lattice (ϕ) along the selected radial directions. The density of points (step) during measurements was 25 nm. It is evident that although the integral dependence $\phi(r)$ has a character close to linear, the dependence is a sequence of relatively sharp jumps in the value of ϕ , followed by a 'shelf' or even a small rotation of the lattice in the opposite direction. This alternation has a fairly regular character, which manifests itself primarily in areas close to the center of the island, with a periodicity of about 0.6–0.8 μ m. Comparison of the periodicity of jumps on the $\phi(r)$ dependence and boundaries associated with circular-step growth suggests that the region of boundaries (crystalline disturbances) corresponds to jumps on the $\phi(r)$ dependence, and the shelves correspond to the regions between these boundaries. The integral rate (gradient) of rotation of the growth axis in the observed island was 0.5–0.6 deg/ μ m.

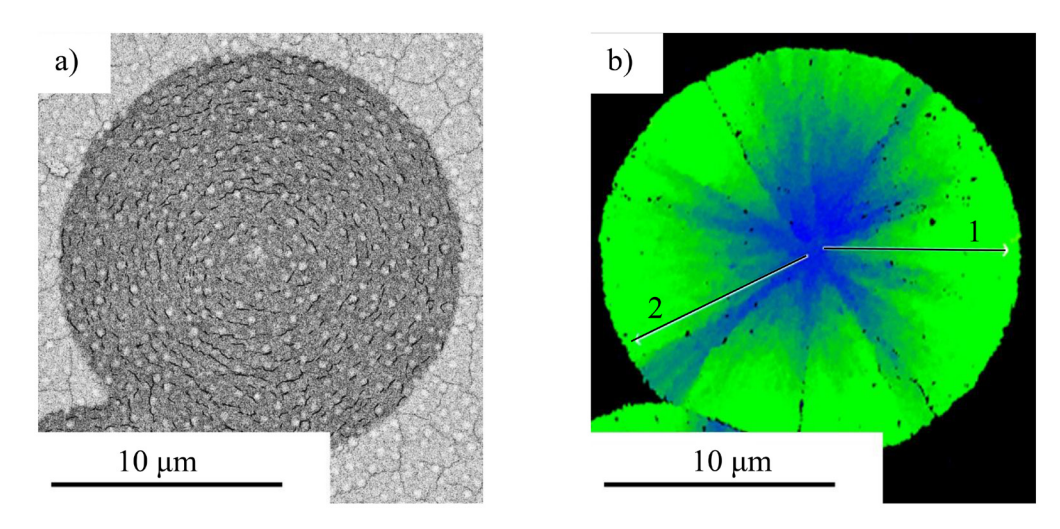
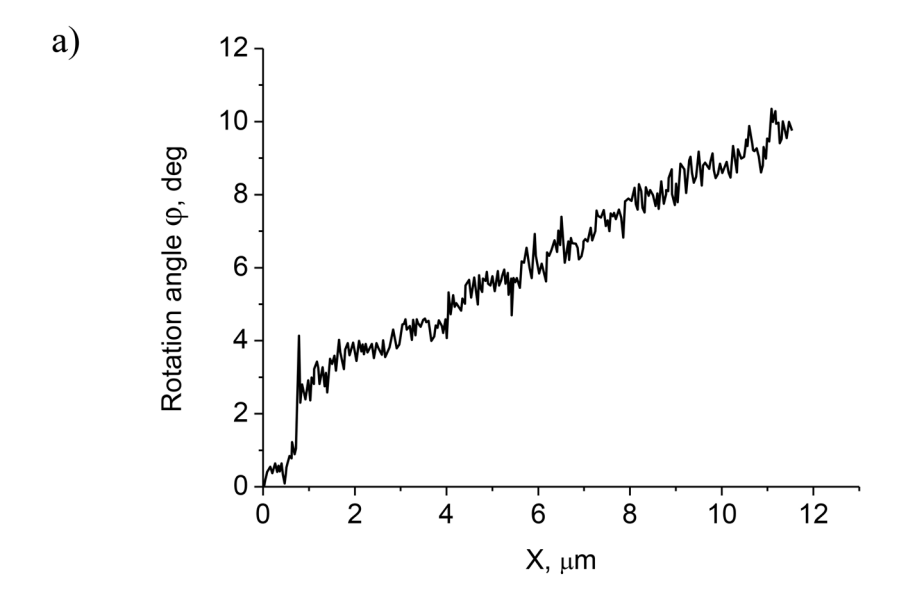


Fig. 1. SEM image (a) and GROD map (b) of the spherulitic island of a PZT film formed on a silicon substrate



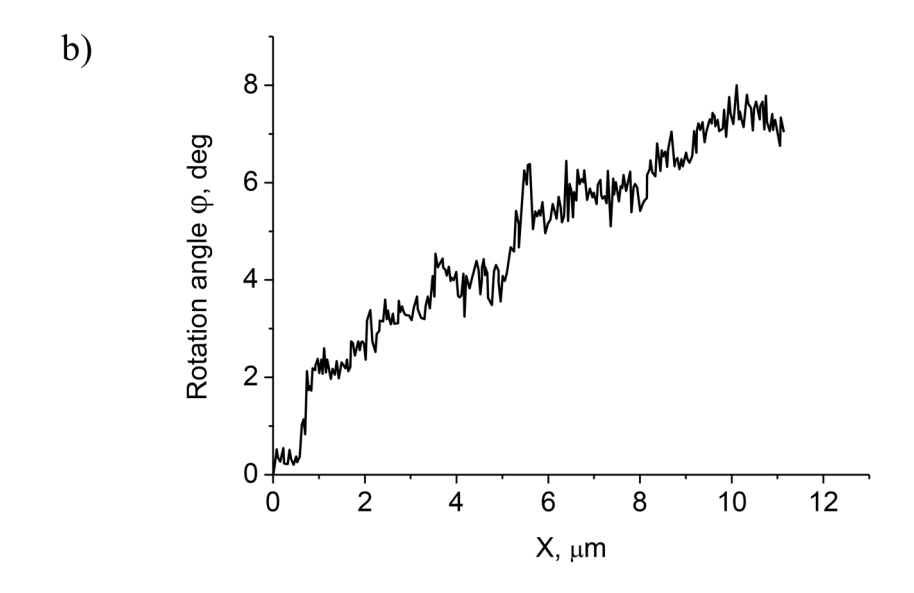


Fig. 2. Change in the rotation angle of the lattice (ϕ) along the radial directions 1 (a) and 2 (b) highlighted in Fig. 1

Fig. 3 shows SEM images of a perovskite island in a PZT film deposited on a sitall substrate, representing a pattern of electron channeling. It was previously noted that BSD patterns of electron channeling are a consequence of low-angle crystalline branching of the islands under study, the crystallization of which occurs under the conditions of the orientational correlation of perovskite grains in the plane of the film (Da et al. 2024). The GROD map indicates an axially uniform rotation angle of the crystal lattice in contrast to the island deposited on a silicon substrate, which is characterized by an axially non-uniform rotation (Fig. 1). The images of lines and nodes reflect the real planes and nodes of the deformed crystal lattice and are caused by its bending (rotation) (Staritsyn et al. 2024). In addition, the BSD picture of the island indicates the absence of circular-step growth. This is confirmed by the dependence $\phi(r)$ shown in Fig. 4, indicating a smooth, jump-free rotation of the lattice. At the same time, the rate of lattice rotation itself is more than two times higher than in an island with a radial-radiant microstructure (Staritsyn et al. 2024), which shows that the mechanisms of lattice rotation in such spherulites are different.

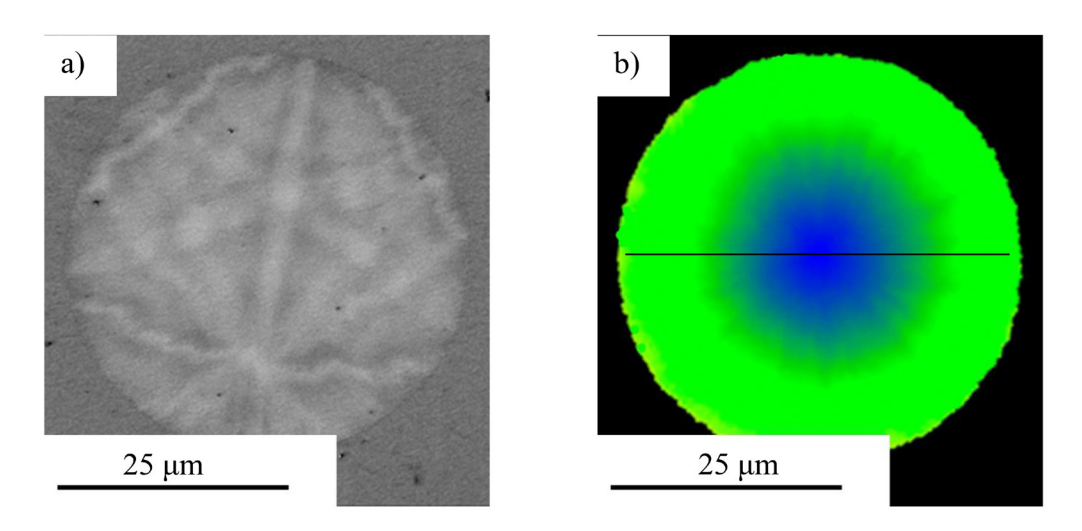


Fig. 3. SEM image (a) and GROD map (b) of the spherulitic island of a PZT film formed on a sitall substrate

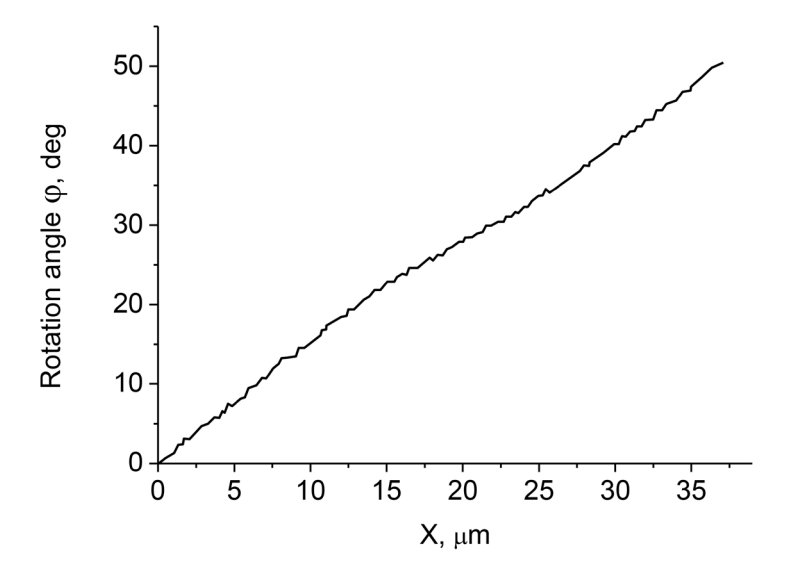


Fig. 4. Changes in the rotation angle of the lattice (ϕ) along the diametrical direction highlighted in Fig. 3

The study of the microstructure of single-phase block thin films showed that the circular-step structure is most clearly manifested in them (Fig. 5). The distances between individual boundaries with an increasing block size are in the same range — at the level of $0.7-0.8 \, \mu m$, as in individual islands.

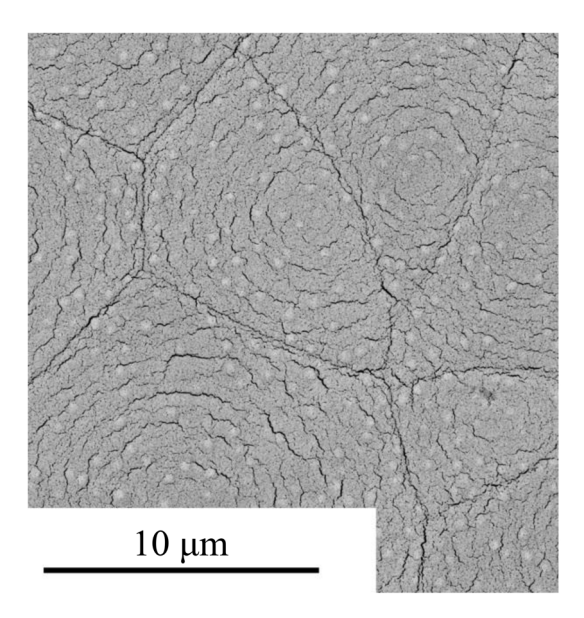


Fig. 5. SEM image of the microstructure of a single-phase block PZT film obtained in the backscattered electron mode

To explain the observed microstructural features of the growth of radial-rayed spherulitic islands and single-phase block films, one should bear in mind that the observed circular and radial boundaries are formed in the course of high-temperature annealing during crystallization of the perovskite phase. Their appearance is caused by the action of tensile mechanical stresses in the plane of the thin film. In this case, radial boundaries are formed as a result of non-crystalline low-angle branching (Da et al. 2024; Shtukenberg et al. 2012), and the formation of circular boundaries is caused, in all likelihood, by the accumulation of elastic deformation, reaching the plastic limit, and the appearance of plastic deformation, leading to both a lattice rotation and relaxation of tensile mechanical stresses. Judging by the nature of the rotation, plastic deformation is realized through the disclination mechanism, accompanied by the appearance of an array of edge dislocations (Savytskii et al. 2016), when the rotation of the crystal lattice occurs abruptly at a sufficiently large angle — in our case, at a value of about 0.7–1.0 degrees (Fig. 6a).

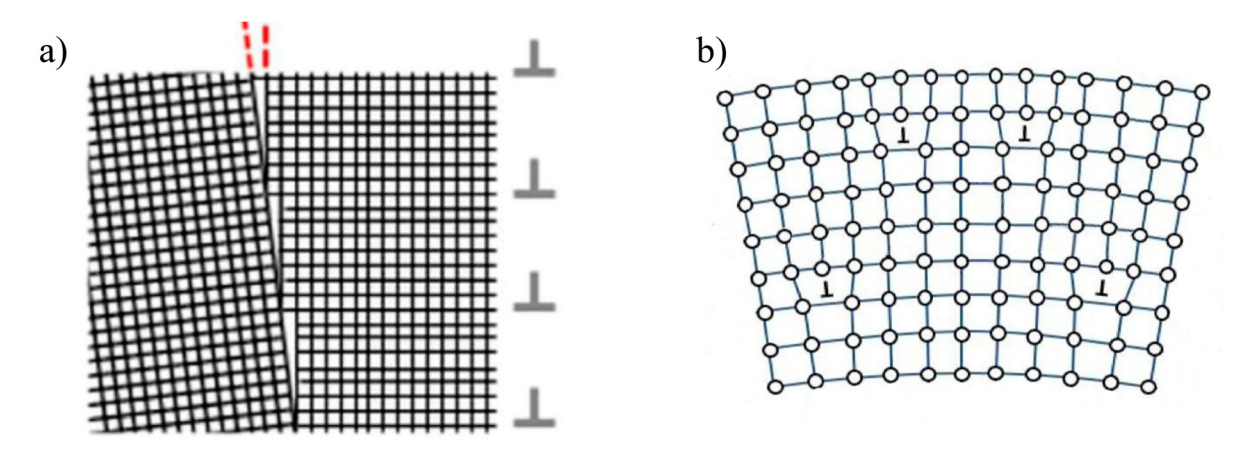


Fig. 6. Schematic representation of the disclination model (a) and lattice bending with the formation of individual edge dislocations (b)

A different mechanism is apparently realized for axially uniform lattice rotation, for which the formation of individual edge dislocations distributed over the area and volume of the thin film is sufficient (Fig. 6b). The formation of edge dislocations requires significantly less energy than the formation of a plastic dislocation, as a result of which the rotation of the crystal lattice can occur quite smoothly, as evidenced by the dependence $\phi(r)$ in Fig. 4.

Conclusion

The experimental data obtained by the scanning electron microscopy study of spherulitic islands characterized by a radial-radiant structure with an axially non-uniform angle of rotation of the lattice and islands characterized by an axially uniform rotation, as well as the results of previous studies and an analysis of the available literature, allowed us to draw the following conclusions.

- 1. Circular-step and radial boundaries are observed in thin-film PZT spherulites, in which the formation of the microstructure is determined by the process of low-angle non-crystalline branching. The presence of boundaries leads to a partial relaxation of lateral mechanical stresses that arise during the crystallization of amorphous films previously deposited on the substrate and a decrease in the rate of rotation of the crystal lattice. It is assumed that in such films, lattice rotation is realized through the disclination mechanism.
- 2. The growth of islands in axially uniformly deformed thin films occurs through low-angle crystalline branching, the microstructure of which is distinguished by the absence of both circular-step and radial boundaries. It is assumed that lattice rotation in such islands occurs through the formation of single edge dislocations.

Conflict of Interest

The authors declare that there is no conflict of interest, either existing or potential.

Author Contributions

The authors have made an equal contribution to the preparation of the paper.

References

- Alkoy, E. M, Alkoy, S., Shiosaki, T. (2007) The effect of crystallographic orientation and solution aging on the electrical properties of sol-gel derived $Pb(Zr_{0.45}Ti_{0.55})O_3$ thin films. Ceramic International, 33 (8), 1455–1462. https://doi.org/10.1016/j.ceramint.2006.06.010 (In English)
- Carim, A. H., Tuttle, B. A., Doughty, D. H., Mrtinz, S. L. (1991) Microstructure of solution-processed lead zirconate titanate (PZT) thin films. Journal of the American Ceramic Society, 74 (6), article 1455. https://doi.org/10.1111/j.1151-2916.1991.tb04130.x (In English)
- Da, B., Cheng, L., Liu, X. et al. (2024) Exploring high-symmetry structures in non-Cartesian coordinates: Preparation and characteristics of cylindrically symmetric-rotating crystals. Science and Technology of Advanced Materials: Methods, 4 (1), article 2406743. https://doi.org/10.1080/27660400.2024.2406743 (In English)
- Krupanidhi, S. B. (1992) Recent advances in the deposition of ferroelectric thin films. Integrated Ferroelectrics, 1 (2-4), 161–180. https://doi.org/10.1080/10584589208215709 (In English)
- Kwok, C. K., Desu, S. B. (1994) Formation kinetics of $PbZr_xTi_{1-x}O_3$ thin films. Journal of Materials Research, 9, 1728–1733. <u>https://doi.org/10.1557/JMR.1994.1728</u> (in English)
- Lutjes, N. R., Zhou, S., Antoja-Lleonart, J. et al. (2021) Spherulitic and rotational crystal growth of Quartz thin films. Scientific Reports, 11 (1), article 14888. https://doi.org/10.1038/s41598-021-94147-y (In English)
- Musterman, E. J., Dierolf, V., Jain, H. (2022) Curved lattices of crystals formed in glass. International Journal of Applied Glass Science, 13 (3), 402–419. https://doi.org/10.1111/jiag.16574 (In English)
- Preston, K. D., Haertling, G. H. (1992) Microstructural investigation of acetate derived PLZT films. Integrated Ferroelectrics, 1, 89–98. https://doi.org/10.1080/10584589208215567 (In English)
- Pronin, I. P. (2017) Formirovanie submikronnykh polikristallicheskikh sloev tsirkonata-titanata svintsa, ikh fazovoe sostoyanie i segnetoelektricheskie svojstva [Formation of submicron polycrystalline layers of lead zirconate titanate, their phase state and ferroelectric properties]. PhD dissertation (Physics). Saint Petersburg, Herzen State Pedagogical University of Russia, 261 p. (In Russian)
- Pronin, I. P., Zaitseva, N. V., Kaptelov, E. Yu., Afanasiev, V. P. (1997) Opticheskij kontrol' odnofaznosti tonkikh polikristallicheskikh segnetoelektricheskikh plenok so strukturoj perovskita [Optical control of phase state of polycrystalline ferroelectric thin films with perovskite structure]. Izvestia AN. Seria Fizicheskaya Bulletin of the Russian Academy of Sciences: Physics, 61, 379–382 (In Russian)
- Pronin, V. P., Ryzhov, I. V., Staritsyn, M. V. et al. (2024) An influence of mechanical stresses on the phase state of spherulitic thin films of lead zirconate titanate. Materials Physics and Mechanics, 52 (6), 17–26 http://dx.doi.org/10.18149/MPM.5262024 3 (In English).
- Pronin, V. P., Senkevich, S. V., Kaptelov, E. Yu., Pronin, I. P. (2010) Features of the formation of a perovskite phase in thin polycrystalline Pb(Zr,Ti)O₃ films. Journal of Surface Investigation. X-ray, Synchrotron and Neutron Techniques, 4, 703–708. https://doi.org/10.1134/S1027451010050010 (In English)

- Savytskii, D., Jain, H., Tamura, N., Dierolf, V. (2016) Rotating lattice single crystal architecture on the surface of glass. Scientific Reports, 6, article 36449. https://doi.org/10.1038/srep36449 (In English)
- Shtukenberg, A. G., Punin, Y. O., Gunn, E., Kahr, B. (2012) Spherulites. Chemical Reviews, 112 (3), 1805–1838. https://doi.org/10.1021/cr200297f (In English)
- Spierings, G. A. C. M., Van Zon, J. B. A., Larsen, P. K., Klee, M. (1993) Influence of platinum-based electrodes on the microstructure of sol-gel and MOD prepared lead zirconate titanate films. Integrated Ferroelectrics, 3 (3), 283–292. https://doi.org/10.1080/10584589308216719 (In English)
- Staritsyn, M. V., Pronin, V. P., Khinich, I. I. et al. (2023) Mikrostruktura sferolitovykh tonkikh plenok tsirkonatatitanata svintsa [Microstructure of spherulitic lead zirconate titanate thin films]. Fizika Tverdogo Tela Physics of the Solid State, 65 (8), 1368–1374. https://doi.org/10.21883/FTT.2023.08.56155.140 (In Russian)
- Staritsyn, M. V., Pronin, V. P., Khinich, I. I. et al. (2024) Effekt kanalirovaniya elektronov v kristallicheskoj reshetke luchistykh sferolitov [Effect of electron channeling in the crystal lattice of radiant spherulites]. Fiziko-khimicheskie aspekty izucheniya klasterov, nanostruktur i nanomaterialov–Physical and Chemical Aspects of the Study of Clusters, Nanostructures and Nanomaterials, 16, 289–300. https://doi.org/10.26456/pcascnn/2024.16.289 (In Russian)
- Woo, E. M., Lugito, G. (2016) Cracks in polymer spherulites: Phenomenological mechanisms in correlation with ring bands. Polymers, 8 (9), article 329. https://doi.org/10.3390/polym8090329 (In English)



Physics of Semiconductors.
Solid state physics

UDC 538.9 + 535.3

EDN GAMNFT

https://www.doi.org/10.33910/2687-153X-2025-6-3-134-138

Spectra and kinetics of dye-sensitized photovoltaic effect in silicon

M. A. Goryaev^{⊠1}, A. P. Smirnov¹

¹ Herzen State Pedagogical University of Russia, 48 Moika Emb., Saint Petersburg 191186, Russia

Authors

Mikhail A. Goryaev, ORCID: 0000-0002-2182-6763, e-mail: mgoryaev@mail.ru

Alexander P. Smirnov, ORCID: <u>0000-0003-2463-2056</u>, e-mail: <u>veter8808@mail.ru</u>

For citation: Goryaev, M. A., Smirnov, A. P. (2025) Spectra and kinetics of dye-sensitized photovoltaic effect in silicon. *Physics of Complex Systems*, 6 (3), 134–138. https://www.doi.org/10.33910/2687-153X-2025-6-3-134-138 EDN GAMNFT

Received 16 June 2025; reviewed 16 July 2025; accepted 18 July 2025.

Funding: the study did not receive any external funding.

Copyright: © M. A. Goryaev, A. P. Smirnov (2025). Published by Herzen State Pedagogical University of Russia. Open access under CC BY License 4.0.

Abstract. This paper investigates the action of organic dye molecules placed on the surface of semiconductors on the manifestation of the photovoltaic effect in silicon samples with different types of conductivity. Spectral sensitization is observed in the dye absorption band of the photo-EMF for monocrystal samples with n-type conductivity, and a desensitizing effect of the dye is found in samples with p-type conductivity. In addition, the kinetics of the photovoltaic effect in the region of dye absorption in semiconductors with different types of conductivity is different: in n-type silicon, a monotonic increase of the photo-EMF is observed, while in p-type silicon, the photo-EMF first increases and then decreases. In powder samples, effective sensitization of DC photoconductivity is observed for both n-type and p-type semiconductors. The difference of contributions of electrons and holes generated during nonradiative inductive-resonant energy transfer from a dye to a semiconductor to different types of photoelectric effect is discussed.

Keywords: silicon with different types of conductivity, silicon with an adsorbed dye, spectral sensitization, photo-EMF, DC photoconductivity, dye sensitization of photovoltaic effects

Introduction

Spectral sensitization by dyes with an absorption band in the visible and near-infrared spectral region is widely used to increase the sensitivity of photophysical and photochemical processes in various solids (AgHal, ZnO, ${\rm TiO_2}$ and others) (Akimov et al 1980; Goryaev 2015; 2016; 2018; 2019; Goryaev, Pimenov 1975; 1980; James 1977). The application of organic dyes provides effective control of the photosensitivity spectrum and increases the sensitivity of classical silver halide photographic materials (James 1977). Photoelectrochemical cells based on titanium dioxide particles with sensitizing dyes are proposed as an alternative to silicon solar cells (Gratzel 2003). The efficiency of using organic dyes is primarily determined by the high extinction coefficient in the absorption band. One of the significant deficiencies of silicon solar cells is the relatively low extinction coefficient of this semiconductor in the region of indirect transitions; therefore, converters of light energy into electrical energy manufactured on its basis must have a sufficiently large thickness (Alferov et al 2004). Effective dye sensitization of DC photoconductivity was found in powdered silicon (Goryaev 2015; 2016) and in monolithic silicon (Goryaev 2018; 2019). In this paper, the photovoltaic effect in silicon samples with different types of conductivity and the influence of organic dyes on its surface on its spectra and kinetics are investigated.

Results and discussion

The investigations were carried out on samples with electron conductivity, doped with phosphorus at a concentration of 10^{15} cm⁻³, and with hole conductivity, doped with boron at a concentration of 10^{15} cm⁻³. Photo-EMF spectra on flat monocrystalline samples with an area of about 1 cm² and a thickness of $360-450~\mu m$ were measured using the capacitor method (Akimov 1966) at modulated illumination. The block schematic diagram of this measuring complex is shown in Fig. 1.

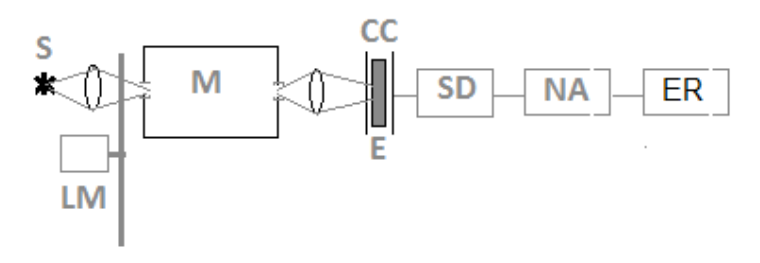


Fig. 1. Block schematic diagram of the laboratory complex for measuring photo-EMF spectra by the capacitor method. S — light source, LM — light modulator, M — monochromator, CC — capacitor cell, E — sample, SD — synchronous detector, NA — narrow-band amplifier, ER — curve-tracer Enregistreur

DC photoconductivity was studied in powdered samples of silicon with a microcrystal size of several microns, obtained by grinding the original single-crystal samples. It was measured in special surface-type cells in order to study the electrophysical properties of powder semiconductors, in which a sample in the form of a tablet is pressed by constant pressure (about 10 kg/cm²) to a quartz plate. Platinum electrodes were applied to a quartz plate in the form of a raster so that the distance between the electrodes was 0.1 mm with an effective electrode length of 80 mm. The ethanol solution of the required dye of a certain concentration was used for placing the dye molecules on the surface of a semiconductor.

The effect of the dye on the photoelectric properties of samples was studied after the adsorption of the dye and the non-stimulated evaporation of the solvent at room temperature. To assess the efficiency of the internal photoelectric effect in different spectral regions, the photo-EMF signals $U_{\rm ph}$ and the DC photocurrents $I_{\rm ph}$ were normalized to the same number of light quanta E falling on the sample. The results, illustrated in Fig. 2, show that the dye applied on the surface of the semiconductors at different concentrations significantly influences the spectra of the capacitor photo-EMF of monocrystal silicon samples with different types of conductivity in the absorption band of the dye.

When rhodamine 6G is placed on the surface of a semiconductor with electronic conductivity, the photo-EMF initially increases with growth dye concentration (Fig. 2a, curves 1 and 2), and spectral sensitization of the photoelectric effect occurs. The maximum value of the recorded signal in the dye absorption band increases almost twofold. The resulting sensitized photoelectric effect is determined by the different contribution of charge carriers generated due to energy transfer from the dye. In silicon, when light is absorbed in a given region, both additional electrons and holes appear when electrons transfer between the valence band and the conduction band. The studied samples were homogeneous. They did not contain heterojunctions, and no conditions for the implementation of the valve component of the photo-EMF were created. Therefore, the observed capacitor photo-EMF has a diffusion nature

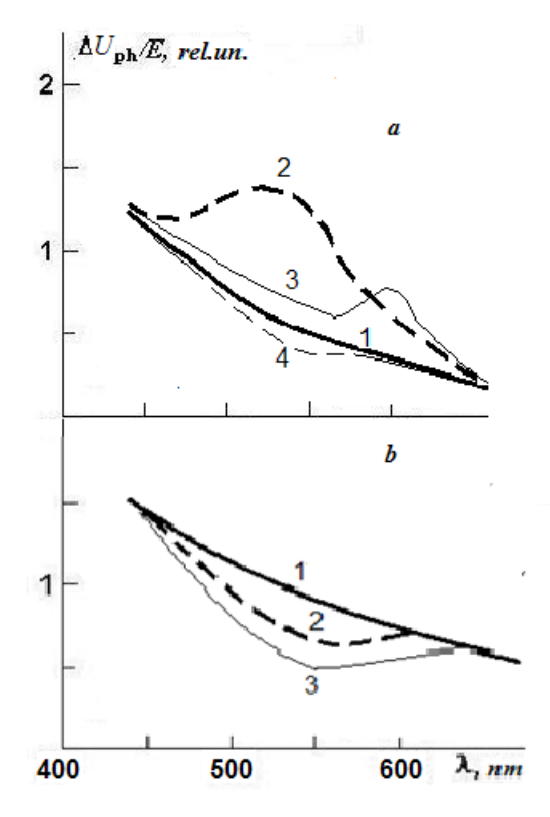


Fig. 2. Photo-EMF spectra of a silicon sample without dye (1) and samples dyed with rhodamine 6G at dye molecule concentrations of 40 nm⁻² (2), 70 nm⁻² (3) and 110 nm⁻² (4); a — n-type semiconductor, b — p-type semiconductor

and is caused by the diffusion of generated charge carriers in the semiconductor due to the gradient of their concentration during light absorption (Dember effect) (Akimov 1966; Bonch-Bruevich, Kalashnikov 1977). The Dember EMF is determined by the relationship:

$$U_{ph} = \frac{kT}{e} \frac{\mu_n - \mu_p}{\mu_n + \mu_p} ln \frac{\sigma_1}{\sigma_2},$$

where μ_n and μ_p are the mobilities of electrons and holes, while σ_1 and σ_2 are the conductivities at the front and back surfaces of the sample. The magnitude of the EMF will be determined by the difference in the mobilities of electrons and holes. In silicon, the mobility of holes is several times lower than that of electrons (Bonch-Bruevich, Kalashnikov 1977); therefore, the main contribution to the change in photo-EMF is made by electrons generated during the transfer of energy from the dye.

In n-type silicon without dye, the photo-EMF is caused by electrons; therefore, when the dye is applied at small concentrations, an increase in the EMF is also observed due to additional electrons appearing as a result of the transfer of photoexcitation energy from the dye to the semiconductor (Fig. 2a, curves 1 and 2). Further, with an increase in the amount of the applied dye, the value of the photo-EMF decreases (Fig. 2a, curves 3 and 4) since part of the energy hitting the sample does not reach the semiconductor due to an increase in the thickness of the dye film on the surface of this semiconductor, and a filter effect is observed in the absorption band of the dye (Goryaev 1980; 2015; 2019).

It should be noted that the filter effect manifests itself primarily in the short-wave region of the dye absorption band (Fig. 2a, curve 3). This is due to the fact that, according to the theory, the efficiency of inductive-resonant nonradiative energy transfer depends on the overlap integral of the luminescence spectrum of the donor and the absorption spectrum of the energy acceptor (Ermolaev et al 1996):

$$K = C \int I_d n(v) \varepsilon_a(v) v^{-4} dv ,$$

where I_d is the quantum spectral density of the donor luminescence radiation, $\varepsilon_a(v)$ is the molar decimal absorption coefficient of the energy acceptor, n is the refractive index of the medium, v is the wave number and C is a constant. The overlap integral strongly depends on the wave number, which is confirmed by the more noticeable luminescence quenching of dyes in the long-wavelength region of the spectrum during the transfer of energy to the solid (Goryaev, Akimov 1979). Therefore, the spectra of the sensitized photoelectric effect are shifted relative to the absorption spectra of the dye, and with an increase in the dye concentration, the filter effect is first noticeable in the short-wave region of the absorption band; in addition, sensitization of the photo-EMF is observed in the long-wave region (Fig. 2a, curve 3) and it is only with a further increase in the dye concentration that merely the filter effect is observed. (Fig. 2a, curve 4).

The magnitude of the photo-EMF of p-type monocrystal silicon samples decreases monotonically from the beginning in the absorption band of the dye if its concentration on the surface of the semiconductor increases (Fig. 2b, curves 1–3). As already noted, the photo-EMF, due to the carriers of the charge generated when the transfer of photoexcitation energy occurs from the dye to the semiconductor is ultimately determined by additional electrons. The polarity of this component is opposite to the photo-EMF caused by the majority charge carriers of p-type silicon, i. e. holes. All this, together with the filter effect described above, leads to a desensitizing effect of the dye on the photovoltaic effect in p-type silicon (Goryaev 2024a; 2024b).

The different influence of the dye on the photovoltaic effect in silicon with different types of conductivity is confirmed by kinetic investigations (Goryaev 2025). Fig. 3 shows kinetic curves of the photo-EMF of n-type (a) and p-type (b) silicon samples upon excitation by light in the absorption band of the dye.

When the dye is applied to the surface of silicon, an increase in the photo-EMF value is observed at low concentrations since the main contribution to the change in EMF is made by the electrons generated during the transfer of energy from the dye and it coincides with polarity of the photo-EMF in the original n-type silicon (Fig. 3a, curves 1 and 2). An increase in the dye concentration is further accompanied by a decrease in the signal (curve 3), associated with a filter effect in the absorption band of the dye.

The photo-EMF of silicon samples with hole conductivity in the steady state decreases in the absorption band of the dye as its concentration on the surface of the semiconductor increases (Fig. 3b, curves 1-3). This is due to the fact that the additional photo-EMF during the transfer of photoexcitation energy from the dye is determined by electrons and its polarity is opposite to the photo-EMF caused by the main

carriers of p-type silicon, which leads to a desensitizing effect of the dye: the photoelectric effect almost completely disappears (curve 3). It should be noted that the kinetic curve of the photovoltaic effect is non-monotonic at a relatively high concentration of the dye (Fig. 3b, curve 3). This behavior may be explained by the fact that the generation of additional carriers due to the transfer of photoexcitation energy from the dye molecule to the semiconductor begins later than carriers appear after direct absorption of light during interband transition in silicon.

The investigation of DC photoconductivity revealed spectral sensitization of powdered silicon samples with both electron and hole conductivity (Fig. 4).

The photoconductivity of n-type semiconductors without dye (Fig. 4a, curve 1) is slightly higher than photoconductivity of p-type samples (Fig. 4b, curve 1), and the photoelectric effect, when a dye is applied, is almost two orders of magnitude higher than the photoconductivity of the original samples (Fig. 4, curves 2). This is due to the fact that both electrons and holes generated when the transfer of photoexcitation energy occurs from the dye to the semiconductor lead to an increase in photoconductivity, and the high efficiency of sensitization is due to the fact that the specific surface area of powdered silicon is several orders of magnitude larger than the specific surface area of monocrystal samples.

Conclusion

The adsorption of an organic dye on the surface of silicon monocrystals provides a sensitizing effect in the dye absorption band on the photovoltaic Dember effect in samples with n-type conductivity and a desensitizing effect in p-type samples. In silicon powder samples, efficient sensitization of DC photoconductivity is observed for semiconductors with both n-type and p-type conductivity. Spectral sensitization with dyes can be used to increase the efficiency of silicon systems for converting light energy into electrical energy, and the identified sensitizing and desensitizing actions of the dye on the photovoltaic effect in silicon with different types of conductivity must be taken into account when complex systems with heterojunctions are created for such semiconductor devices.

Conflict of Interest

The authors declare that there is no conflict of interest, either existing or potential.

Author Contributions

The authors have made equal contributions to the paper.

Acknowledgements

The authors are grateful to V. G. Kossov and V. A. Ivanov for providing the silicon samples.

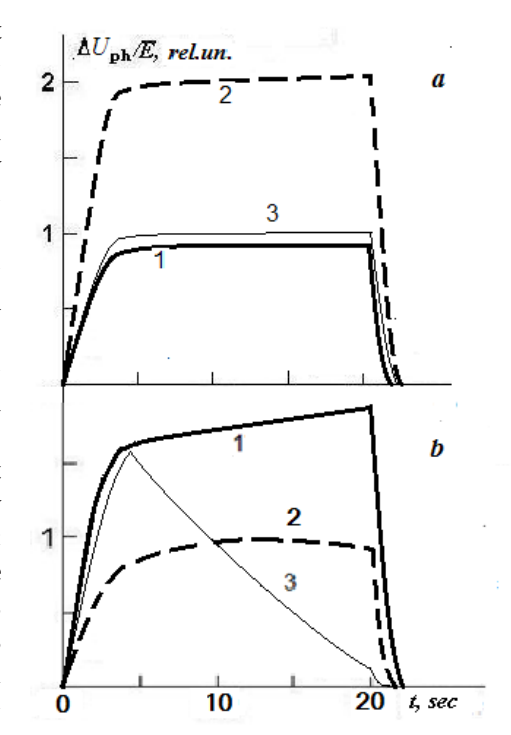


Fig. 3. Kinetics of the photovoltaic effect in silicon without dye (1) and in samples dyed with rhodamine 6G with dye molecule concentrations of 40 nm⁻² (2) and 70 nm⁻² (3); a — n-type semiconductor, b — p-type semiconductor

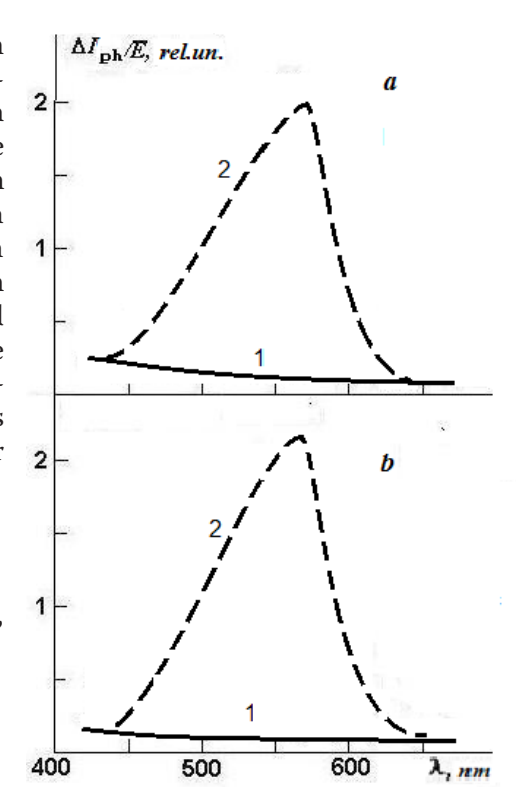


Fig. 4. Photoconductivity spectra of silicon without dye (1) and samples dyed with rhodamine 6G with a dye molecule concentration of 10⁻⁴ mol/gSi (2); a — n-type semiconductor, b — p-type semiconductor

References

- Akimov, I. A. (1966) The Internal photoeffect investigation in semiconductors by the condenser method. *Soviet Journal of Optical Technology*, 33 (5), 248–255. (In English)
- Akimov, I. A., Cherkasov, U. A., Cherkashin, M. I. (1980) Sensibilizirovannyj fotoeffekt [Sensitized photoeffect]. Moscow: Nauka Publ., 384 p. (In Russian)
- Alferov, J. I., Andreev, V. M., Rumyantsev, V. D. (2004) Solar photovoltaics: Trends and prospects. *Semiconductors*, 38 (8), 899–908. (In English)
- Bonch-Bruevich, V. L., Kalashnikov S. G. (1977) Fizika poluprovodnikov [Physics of Semiconductors]. Moscow: Nauka Publ., 672 p. (In Russian)
- Ermolaev, V. L., Sveshnikova, E. B., Bodunov, E. N. (1996) Inductive-resonant mechanism of nonradiative transitions in ions and molecules in condensed phase. *Physics-Uspekhi*, 39 (3), 261–282. https://doi.org/10.1070/pu1996v039n03abeh000137 (In English)
- Goryaev, M. A. (1980) Photoprocesses in aluminum hydride with adsorbed dye. *Optics and Spectroscopy*, 49 (6), 625–627. (In English)
- Goryaev, M. A. (2015) Dye sensitization of photoconductivity of polycrystalline silicon. *Russian Journal of Physical Chemistry A*, 89 (12), 2320–2321. (In English)
- Goryaev, M. A. (2016) Sensitized photoconductivity in silicon. In: 13th International scientific-technical conference on actual problems of electronic instrument engineering (APEIE) 39281: Proceedings. Novosibirsk: Novosibirsk State Technical University Publ., pp. 24–26 (In English)
- Goryaev, M. A. (2018) Sensitized photovoltaic effect in silicon. In: 14th International scientific-technical conference on actual problems of electronic instrument engineering (APEIE) 44894: Proceedings. Novosibirsk: Novosibirsk State Technical University Publ., pp. 13–15. https://doi.org/10.1109/APEIE.2018.8545466 (In English)
- Goryaev, M. A. (2019) Spectral sensitization of Photo-EMF in monocrystalline silicon. *Optics and Spectroscopy*, 127 (1), 167–169 (In English)
- Goryaev, M. A. (2024a) Dye insluence on Photo-EMF in n- and p-type silicon. In: *XIII International Conference on Photonics and Information Optics Proceedings*. Moscow: MIFI Publ., pp. 271–272. (In Russian)
- Goryaev, M. A. (2024b) Dye-sensitized photoprocesses in Silicon. In: *XVI International Conference "Dielectrics-2024" Proceedings*. Saint Petersburg: the Herzen State Pedagogical University of Russia, p. 16. (In Russian)
- Goryaev, M. A. (2025) Kinetics of dye-sensitized photoprocesses in n- and p-type silicon. In: *XIV International Conference on Photonics and Information Optics Proceedings.* Moscow: MIFI Publ., pp. 333–334. (In Russian)
- Goryaev, M. A., Akimov, I. A. (1979) Luminescence of dyes adsorbed on aluminum hydride and its variation during photolysis of the adsorbent. *Optics and Spectroscopy*, 47 (2), 229–230 (In English)
- Goryaev, M. A., Pimenov, Y. D. (1975) The action of an electric field on photochemical processes in aluminum hydride. *Soviet Journal of Optical Technology*, 42 (9), 538–541. (In English)
- Goryaev, M. A., Pimenov, Y. D. (1980) Upravlenie protsessami formirovaniya izobrazheniya v neorganicheskikh materialakh [Control of image formation processes in inorganic materials]. *Uspekhi nauchnoj fotografii*, 20, 96–105. (In Russian)
- Gratzel, M. (2003) Dye-sensitized solar cells. *Journal of Photochemistry and Photobiology C: Photochemistry Reviews*, 4 (2), 145–153. https://doi.org/10.1134/S0036024415120146 (In English)
- James, T. H. (1977) The Theory of the Photographic Process. New York: Macmillan Publ., 562 p. (In English)



Physics of Semiconductors.
Solid state physics

UDC 538.91

EDN SANBNC

https://www.doi.org/10.33910/2687-153X-2025-6-3-139-143

Analysis of the local structure of the nearest environment of germanium atoms in chalcogenide alloys $Ge_2Sb_2Te_5$ using the Mössbauer spectroscopy method

A. V. Marchenko¹, Yu. A. Petrushin¹, P. P. Seregin¹, V. A. Doronin ^{⊠2}

Herzen State Pedagogical University of Russia, 48 Moika Emb., Saint Petersburg 191186, Russia
 Mozhaisky Military Space Academy, 13 Zhdanovskaya Str., Saint Petersburg 197198, Russia

Authors

Alla V. Marchenko, ORCID: 0000-0002-9292-2541, e-mail: al7140@rambler.ru

Yuri A. Petrushin, e-mail: <u>uraordie@mail.ru</u>

Pavel P. Seregin, ORCID: 0000-0001-5004-2047, e-mail: ppseregin@mail.ru

Vyacheslav A. Doronin, ORCID: 0009-0007-3185-7903, e-mail: doroninslava@rambler.ru

For citation: Marchenko, A. V., Petrushin, Yu. A., Seregin, P. P., Doronin, V. A. (2025) Analysis of the local structure of the nearest environment of germanium atoms in chalcogenide alloys Ge₂Sb₂Te₅ using the Mössbauer spectroscopy method. *Physics of Complex Systems*, 6 (3), 139–143. https://www.doi.org/10.33910/2687-153X-2025-6-3-139-143 EDN SANBNC

Received 9 April 2025; reviewed 4 May 2025; accepted 26 June 2025.

Funding: the study did not receive any external funding.

Copyright: © A. V. Marchenko, Yu. A. Petrushin, P. P. Seregin, V. A. Doronin (2025). Published by Herzen State Pedagogical University of Russia. Open access under <u>CC BY License 4.0</u>.

Abstract. The tetrahedral symmetry of the local environment of germanium atoms in amorphous $Ge_2Sb_2Te_5$ films has been demonstrated by Mössbauer spectroscopy in a ^{73}Ge isotope. We conclude that there is a significant difference in the immediate environment and, consequently, in the electronic structures of Ge atoms in crystalline and amorphous $Ge_2Sb_2Te_5$ films. X-ray amorphous $Ge_2Sb_2Te_5$ films with a thickness of 20 μ m were obtained by magnetron sputtering of synthesized polycrystalline samples at direct current in a nitrogen atmosphere onto aluminum foil substrates. The films were then annealed in the temperature range of 150–200 °C to obtain polycrystalline samples. The composition of the films was controlled by X-ray fluorescence analysis.

 $\textit{Keywords:}\ \text{M\"ossbauer}\ \text{spectroscopy},\ \text{Ge}_2\text{Sb}_2\text{Te}_5,\ \text{local environment of Ge, magnetron sputtering, X-ray fluorescence analysis}$

Introduction

Phase transition materials based on $\mathrm{Ge_2Sb_2Te_5}$ chalcogenide alloys (GST) are widely used for data storage and encoding. To develop new materials that meet the requirements of high density and miniaturization of storage devices, one should understand the details of their microstructure and related distortions in both crystalline and amorphous states. Based on the *X*-ray absorption fine structure spectroscopy (*EXAFS*) study, it was believed that the amorphization of the GST alloy under laser radiation is accompanied by a jump of the germanium atom from octahedral positions occupied in the crystal to tetrahedral positions, and in both phases the Ge and Sb atoms are bound only to Te atoms (Kolobov et al. 2004). Using the same method, amorphous GST obtained by sputtering revealed a significant proportion of Ge–Ge bonds in addition to the usual Ge–Te bonds (Baker et al. 2006). Based on the results of modeling from the first principles of amorphous GST obtained by quenching from the liquid phase, Caravati S. and Bernasconi M. found out that one third of the Ge atoms in its structure are in a tetrahedral

environment, while the remaining Ge, Sb, and Te atoms have a defective octahedral environment, reminiscent of the environment of these atoms in crystalline GST (Caravati, Bernasconi 2007). Liu X. et al. demonstrated the coexistence of octahedral and tetrahedral coordinated germanium cations in the structure of crystalline GST using high-resolution transmission electron microscopy and X-ray diffraction, with the proportion of tetrahedral Ge to the total amount of Ge ranging from 0.32 to 0.37 for different samples (Liu et al. 2011). Using the principles of molecular dynamics within the framework of density functional theory, A. Bouzid et al. established that in the structure of glassy GST, Ge atoms are located in a tetrahedral grid, although a considerable proportion of Ge atoms are also found in defective octahedra, with tetrahedra clearly predominating (Bouzid et al. 2017). Finally, in J. Stellhorn et al., anomalous X-ray scattering revealed that approximately half of the Ge atoms in the amorphous GST phase have an octahedral environment similar to that in a crystal, while the remaining part of the Ge atoms with tetrahedral symmetry acts as an energy barrier between the phases, ensuring a long lifetime of amorphous GST (Stellhorn et al. 2020).

The existing contradictions in the interpretation of the experimental results indicate the need to use experimental methods that are more sensitive to minor changes in the electronic structure of atoms during the phase transition from an amorphous to a crystalline state. Mössbauer spectroscopy (MS) on isotopes 125 Te, 121 Sb, and 119 Sn proved to be an effective tool for detecting changes in the local environment of atoms and their electronic structure during amorphization of the $Ge_2Sb_2Te_5$ compound (Marchenko et al. 2023). In particular, the Mössbauer study on the 119 Sn impurity probe led us to a conclusion that the symmetry of the local environment of germanium atoms changed during the crystal-amorphous transition in the $Ge_2Sb_2Te_5$ alloy. However, this conclusion was based on assumptions about the isovalent substitution of germanium atoms with tin atoms in crystalline and amorphous films.

That is why it seemed advisable to study the local structure of the germanium atom layer in amorphous $\mathrm{Ge_2Sb_2Te_5}$ alloy films using MS on $^{73}\mathrm{Ge}$ atoms. However, it should be noted that despite the fundamentally great possibilities of MS based on the $^{73}\mathrm{Ge}$ isotope for studies of this kind, publications on this isotope are scarce due to the problems associated with the difficulties of registering various valence states of germanium in one experimental spectrum.

Pfeiffer and Kovacs performed the first calibration of the isomeric shift of the 73 Ge spectra using a Ge: 73 As source and a 73 Ge monocrystalline absorber (Pfeiffer, Kovacs 1981). Later, Pfeiffer et al. observed the Mössbauer effect for 73 Ge nuclei introduced into the lattice sites of Si and Ge single crystals during laser irradiation (Pfeiffer et al. 1983), concluding that the isomeric shift of the Si: 73 As spectrum relative to the Ge: 73 As spectrum is so large that it casts doubt on their own calibration of the 73 Ge isomeric shift performed in (Pfeiffer, Kovacs 1981). In this regard, A. Svane calculated the electron densities on Ge nuclei in the nodes of Ge and Si crystals (Svane 1988) and, using experimental isomeric shifts from (Pfeiffer et al. 1983), obtained the calibration coefficient $\alpha = 0.74$ mm s⁻¹ a_0^{-3} for the isomeric transition of 13.3 keV to 73 Ge, where a_0^{-1} is the Bohr radius. This result gives hope of a record sensitivity of the position of the 73 Ge spectral line to small changes in the electronic structure.

However, when calculating the α coefficient in (Svane 1988), the value of the Si:⁷³As isomeric shift relative to Ge:⁷³As was assumed to be IS = $-685 \, \mu \text{m/s}$, although in (Pfeiffer et al. 1983) the value of the opposite sign is given. This created an additional motive for our investigation of the local structure of the near germanium atoms in amorphous Ge₂Sb₂Te₅ alloy films. When discussing our results, we will use both IS signs.

Experimental technique

The compound $Ge_2Sb_2Te_5$ was synthesized from elementary substances in quartz ampoules evacuated to 10^{-3} mmHg at 1050 °C. The synthesis used the isotope ^{73}Ge with an e enrichment of 70%. X-ray amorphous $Ge_2Sb_2Te_5$ films with a thickness of 20 μ m were obtained by magnetron sputtering of synthesized polycrystalline samples at direct current in a nitrogen atmosphere onto aluminum foil substrates. The films were then annealed in the temperature range of 150-200 °C to obtain polycrystalline samples. The composition of the films was controlled by *X*-ray fluorescence analysis.

The radioactive isotope 73 As for the preparation of the Mössbauer source was obtained by the reaction 74 Ge(p, 2n) 73 As. The Mössbauer sources Ge: 73 As were prepared on the basis of a Ge monocrystalline film (73 As diffusion in a hydrogen stream at 800 °C for 20 hours). The Mössbauer spectra were measured with a CM 4201 TerLab spectrometer.

Experimental results and their discussion

The Mössbauer spectra of amorphous and polycrystalline $Ge_2Sb_2Te_5$ films are shown in Fig. 1. We can see that the experiment made it possible to register only the spectrum of an amorphous absorber with an isomeric shift of -95(15) µm/s relative to the $Ge:^{73}As$ source in the selected Doppler velocity range.

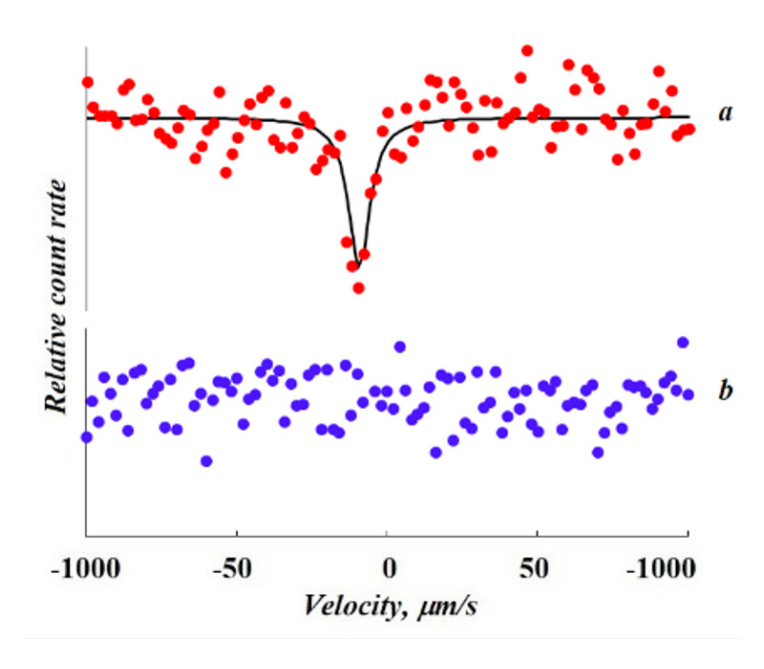


Fig. 1. Mössbauer 73 Ge spectra of amorphous (a) and polycrystalline (b) $\mathrm{Ge_2Sb_2Te_5}$ films at 295 K with a $\mathrm{Ge:^{73}As}$ source

Thus, the expected advantage of the high sensitivity of MS on the Ge^{73} isotope to changes in the electronic structure translated into experimental difficulties. However, the fact that only the spectrum of an amorphous absorber is recorded with the Ge^{73} As source indicates the proximity of the electronic structures of 73 Ge atoms in monocrystalline germanium (the atoms have a tetrahedral chemical bond system) and in the amorphous $Ge_2Sb_2Te_5$ alloy. This confirms the conclusion based on the MS data on 119 Sn impurity atoms about the stabilization of germanium atoms in the amorphous $Ge_2Sb_2Te_5$ alloy in tetrahedral coordination (Marchenko et al. 2023). It also indirectly confirms the conclusion (Marchenko et al. 2023) that there is a significant difference in the immediate environment and, consequently, the electronic structures of Ge atoms in crystalline and amorphous $Ge_2Sb_2Te_5$ films.

An attempt was made to establish correlations between the isomeric shifts of both Mössbauer isotopes to assess the possible position of the ⁷³Ge spectrum in the crystal film and to jointly interpret the MS results for the ⁷³Ge and ¹¹⁹Sn isotopes. Calculations of the electron densities on the nuclei of Ge and Sn impurities in the same matrices, which show a linear correlation between these values, are a prerequisite for their search (Svane 1988).

In Fig. 2, these data are plotted on the axes isomeric shift 73 Ge (relative to crystalline Ge) IS $_{\rm Ge}$ — isomeric shift 119 Sn (relative to α -Sn) IS $_{\rm Sn}$ in silicon, germanium and copper matrices. Experimental data for 73 Ge are taken from (Pfeiffer, Kovacs 1981; Pfeiffer et al. 1983) and for 119 Sn from (Regel, Seregin 1984). In this case, the values of the 73 Ge isomeric shift in Si are plotted with both signs, as discussed above. They can be approximated by two linear functions:

$$IS_{Ge} (\mu m/s) = 2309 \times IS_{Sn} (mm/s) + 43.3$$
 (1)

$$IS_{Ge} (\mu m/s) = -2583 \times IS_{Sn} (mm/s) - 152.4$$
 (2)

The dotted line corresponds to the ratio (2) and the isomeric shift of 73 Ge in Si IS $_{Ge} = -685 \, \mu m/s$, while the solid line represents the ratio (1) and the isomeric shift of 73 Ge in Si IS $_{Ge} = +685 \, \mu m/s$.

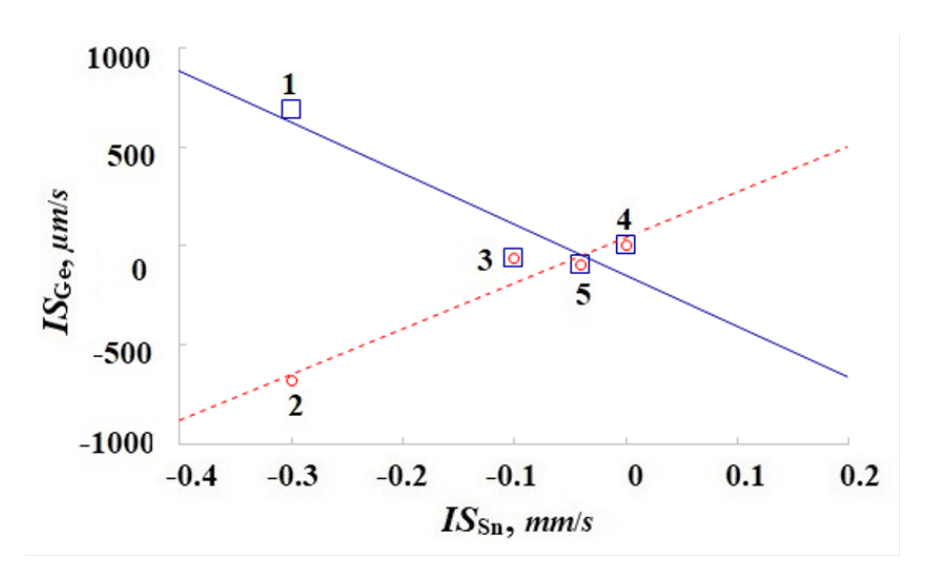


Fig. 2. Relations between isomeric shifts of the Mössbauer spectra of ^{119}Sn IS $_{Sn}$ atoms (circles) and ^{73}Ge IS $_{Ge}$ (squares) in monocrystalline silicon (1, 2), copper (3), germanium (5), and in an amorphous $Ge_2Sb_2Te_5$ film (4). Experimental data for ^{73}Ge are taken from (Pfeiffer, Kovacs 1981; Pfeiffer et al. 1983) and for ^{119}Sn from (Regel, Seregin 1984). The dotted line corresponds to the ratio (2) and the isomeric shift of ^{73}Ge in Si IS $_{Ge}=-685~\mu m/s$, while the solid line represents the ratio (1) and the isomeric shift of ^{73}Ge in Si IS $_{Ge}=+685~\mu m/s$

Thus, the choice of one of the ratios (1) or (2) is of no fundamental importance for estimating the range of assumed positions of the ^{73}Ge spectrum to the $Ge_2Sb_2Te_5$ crystal film. However, it may be important in determining the nuclear characteristics of ^{73}Ge . In particular, Svane assumed the ^{73}Ge isomeric shift in Si to be $-685~\mu m/s$, which corresponds to the ratio (2), and obtained a relative change in the charge radius upon transition to the level of 13.3 keV $\Delta R/R = 1.7 \times 10^{-3}$. If we use the value of the isomeric shift of ^{73}Ge in Si equal to +685 $\mu m/s$, then it leads to the ratio (1), which definitely indicates that the value of $\Delta R/R$ for ^{73}Ge should be considered equal to -1.9×10^{-3} .

Conclusions

Using Mössbauer spectroscopy on the ⁷³Ge isotope, we demonstrated the tetrahedral symmetry of the local environment of germanium atoms in amorphous Ge₂Sb₂Te₅ films, concluding that there is a significant difference both in the local symmetry of the nearest environment of germanium atoms and in their electronic structure in crystalline and amorphous Ge₂Sb₂Te₄ films.

The possibility of one of two relationships between the isomeric shifts of the Mössbauer spectra of ^{73}Ge and ^{119}Sn atoms in silicon, germanium, and copper has been established. Both ratios give the same absolute value of the isomeric shift of the Mössbauer ^{73}Ge spectrum in an IS $_{\text{Ge}}$ polycrystalline film but at the same time lead to either its positive or negative sign. If we take IS $_{\text{Ge}}$ to be negative, then the relative change in the ^{73}Ge charge radius upon transition to the 13.3 keV level turns out to be equal to $\Delta R/R = 1.7 \times 10^{-3}$. If we use a positive IS $_{\text{Ge}}$ value, then the value of $\Delta R/R$ turns out to be equal to -1.9×10^{-3} .

Conflict of Interest

The authors declare that there is no conflict of interest, either existing or potential.

Author Contributions

A. V. Marchenko and P. P. Seregin formulated the research problem. V. A. Doronin synthesized the samples. Yu. A. Petrushin organized the measurement and processing of the experimental spectra. All authors contributed equally to the work by discussing the results and collaborating on writing the article.

References

- Baker, D. A., Paesler, M. A., Lucovsky, G. et al. (2006) Application of bond constraint theory to the switchable optical memory material Ge₂Sb₂Te₅. *Physical Review Letters*, 96, article 255501. https://doi.org/10.1103/ PhysRevLett.96.255501 (In English)
- Bouzid, A., Ori, G., Boero, M. (2017) Atomic-scale structure of the glassy $Ge_2Sb_2Te_5$ phase change material: A quantitative assessment via first-principles molecular dynamics. *Physical Review B*, 96, article 224204. https://doi.org/10.1103/PhysRevB.96.224204 (In English)
- Caravati, S., Bernasconi, M. (2007) Coexistence of tetrahedral- and octahedral-like sites in amorphous phase change materials. *Applied Physics Letters*, 91, article 171906. https://doi.org/10.1063/1.2801626 (In English)
- Kolobov, A., Fons, P., Tominaga, J. et al. (2004) Understanding the phase-change mechanism of rewritable optical media. *Nature Materials*, 3 (10), 703–708. http://dx.doi.org/10.1038/nmat1215 (In English)
- Liu, X. Q., Li, X. B., Zhang, L. et al. (2011) New structural picture of the Ge2Sb₂Te₅ phase-change alloy. *Physical Review Letters*, 106, article 025501. https://doi.org/10.1103/PhysRevLett.106.025501 (In English)
- Marchenko, A. V., Terukov, E. I., Nasredinov, F. S. et al. (2023) Local structure of amorphous (GeTe)x(Sb₂Te₃) films. *Technical Physics*, 68 (1), S88–S95. https://doi.org/10.1134/S1063784223090104 (In English)
- Pfeiffer, L., Kovacs, T. (1981) Calibration of the isomer shift and measurement of $\Delta R/R$ for the 13-keV Mössbauer transition of ⁷³Ge. *Physical Review B*, 23, 5725–5728. https://doi.org/10.1103/PhysRevB.23.5725 (In English)
- Pfeiffer, L., Kovacs, T., Celler, G. K. (1983) Mössbauer effect of ⁷³Ge in laser-processed Si and Ge crystals. *Physical Review B*, 27, 4018–4026. https://doi.org/10.1103/PhysRevB.27.4018 (In English)
- Regel, A. R., Seregin, P. P. (1984) Mössbauer studies of impurity atoms in semiconductors. *Soviet Physics. Semiconductors*, 18, 723–740. (In English)
- Stellhorn, J. R., Hosokawa, S., Kohara, S. (2020) Local- and intermediate-range structures on ordinary and exotic phase-change materials by anomalous X-ray scattering. *Analytical Sciences*, 36 (1), 5–9. http://dx.doi.org/10.2116/analsci.19SAR02 (In English)
- Svane, A. (1988) Electronic structures and isomer shifts of Ge, Sn and Sb impurities in elemental semiconductors. *Journal of Physics C: Solid State Physics*, 21 (31), article 5369. https://doi.org/10.1088/0022-3719/21/31/008 (In English)



Physics of Semiconductors.
Solid state physics

UDC 538.9

EDN RBTYMA

https://www.doi.org/10.33910/2687-153X-2025-6-3-144-149

Composition, structure and properties of PbSb₂Te₄ crystals grown by the Chokhralsky method

S. A. Nemov¹, V. D. Andreeva², A. Yu. Aliabev^{⊠1}

Saint Petersburg Electrotechnical University named after V. I. Ulyanov (Lenin),
 5F Professora Popova Str., Saint Petersburg 197022, Russia
 Peter the Great Saint-Petersburg State Polytechnical University,
 29 B Politekhnicheskaya Str., Saint Petersburg 195251, Russia

Authors

Sergei A. Nemov, ORCID: 0000-0001-7673-6899, e-mail: nemov_s@mail.ru

Valentina D. Andreeva, e-mail: <u>avd2007@bk.ru</u> Aleksei Yu. Aliabev, e-mail: alyabjev au@mail.ru

For citation: Nemov, S. A., Andreeva, V. D., Aliabev, A. Yu. (2025) Composition, structure and properties of $PbSb_2Te_4$ crystals grown by the Chokhralsky method. *Physics of Complex Systems*, 6 (3), 144–149. https://www.doi.org/10.33910/2687-153X-2025-6-3-144-149 EDN RBTYMA

Received 25 June 2025; reviewed 16 July 2025; accepted 18 July 2025.

Funding: the study did not receive any external funding.

Copyright: © S. A. Nemov, V. D. Andreeva, A. Yu. Aliabev (2025). Published by Herzen State Pedagogical University of Russia. Open access under <u>CC BY License 4.0</u>.

Abstract. This paper presents the results of X-ray diffraction and electrophysical studies of PbSb $_2$ Te $_4$ crystals grown by the Chokhralsky method. The phase composition and crystal structure of ingots, including those doped with a donor admixture of copper, are discussed from the qualitative and quantitative perspectives. The samples are a periodic structure. They are multiphase, with PbSb $_2$ Te $_4$ and Sb $_2$ Te $_3$ as dominant phases. The presence of intrinsic electrically active point defects causes a high concentration of holes p $\approx 3.2 \times 10^{20}$ cm $^{-3}$. The temperature dependences of the kinetic coefficients indicate a complex structure of the valence band. Impurity atoms occupy vacancies in the metal sublattice during alloying and form chemical compounds with Sb and Te atoms.

Keywords: semiconductor, PbSb₂Te₄, thermoelectricity, topology insulator, tetradymites, doping, kinetic coefficients, nanocomposites, X-Ray diffraction analysis, temperature dependences of the Hall coefficient, valence band structure

Introduction

The research and development of materials exhibiting unique electronic properties is the most intensively developing field of solid-state physics. The integration of such materials into high-tech industries is the key to creating a new generation of devices with improved performance compared to existing ones.

A group of narrow-bandgap semiconductors with band gap inversion, so-called three-dimensional topological insulators (TI), is one of new electronics materials. These materials are characterized by the properties of an insulator (or semiconductor) in bulk, along with gapless states on the surface, which ensure the flow of spin-polarized current across the surface without energy loss. The use of unusual properties of the TI surface is promising in spintronic, magnetoelectric devices and for the quantum computing (Jayan Rakesh 2022; Wang et al. 2016).

Among the currently discovered materials with TI properties, binary layered compounds Bi_2Te_3 , Bi_2Se_3 and Sb_2Te_3 are the most studied, both experimentally (Chen et al. 2009) and theoretically (Aguilera et al. 2013). A promising area of search for new materials with the ability to control their electronic structure are triple and quadruple compounds based on chalcogenides. Triple-layered tetradymite-like compounds $PbSb_2Te_4$ from the quasi-binary $A^{IV}B^{VI}$ - A^VB^{VI} system (A^{IV} — Ge, Sn, Pb; A^V — Bi, Sb; B^{VI} — Te, Se) are of particular interest. In such compounds, which have a layered structure formed by septuple layers, protected surface states can be localized in both surface and subsurface blocks (Hattori et al. 2023).

In addition, $PbSb_2Te_4$ could be used as a potential material for thermoelectric energy conversion. This material is the result of synthesis based on two main components of low- and medium-temperature thermoelectrics respectively, lead telluride PbTe and antimony telluride Sb_2Te_3 . For effective utilization of such compound as a topological insulator and for thermoelectric energy conversion, a detailed study of the features of its electronic structure and current carrier scattering mechanisms is needed.

Modern theoretical calculations of the energy spectrum of ideal crystals are also important for assessing the potential use of these materials.

Papers studying the electronic structure of TI using first principles theoretical methods are most widely presented in literature (Menshchikova et al. 2013). Electronic structure is usually calculated using the formalism of density functional theory by the pseudopotential method and the full-potential method of linearized coupled plane waves. A generalized gradient approximation describes the exchange-correlation energy, taking into account scalar-relativistic corrections. The spin-orbit interaction is considered by the method of the second variation.

However, theoretical calculations do not take into account the characteristics of the grown tetradymite-like crystals. The high concentration of point defects, including vacancies along with the structural and phase complexity of massive samples obtained by the Czochralski peritectic reaction method, has a significant impact on the actual location of the Fermi level. It is also known that the gaps between septuple layers can serve as natural 'containers' for the accumulation of impurities during synthesis, which leads to fluctuations in their geometric dimensions. The magnitude of the fluctuation depends on the type of impurity and on the presence of conglomerates of impurity atoms in the gap. That is why the electronic structure of real PbSb $_2$ Te $_4$ crystals cannot be understood without an experimental study of their structure and electrophysical properties.

Objects of research

The paucity of investigations into our material can be explained by the technological difficulties of obtaining it. The synthesis of crystals occurs through the peritectic reaction $PbSb_2Te_4 \rightleftharpoons PbTe + Sb_2Te_3$ and is complicated by the need to maintain an equilibrium in a narrow temperature range. The first small samples of layered composite material were grown using the vertical Bridgman method by the team of L. E. Shelimova at the A. A. Baykov Institute of Metallurgy of the Russian Academy of Sciences (Shelimova et al. 2004). The Chokhralsky method with continuous feeding of the synthesized crystal made it possible to obtain samples of a larger size and higher perfection in the direction of the trigonal axis ($\overline{3}$). Cylindrical crystals with a diameter of 20 to 30 mm and a length of about 50–100 mm were grown in the direction of growth. Sufficiently large ingots were cut into samples up to $4\times4\times20$ mm in size and oriented, respectively, in the cleavage plane and along the direction of the inversion-rotary axis $\overline{3}$. Cu-doped samples with (PbTe+Sb₂Te₃)_{0.9995}Cu_{0.0005} and (PbTe+Sb₂Te₃)_{0.9995}Cu_{0.001} stoichiometry were also grown and later investigated.

Experimental results and their discussion

The obtained compounds were initially examined by the X-ray diffraction of the single crystal planes using an automatic diffractometer DRON-UM (CuKa-radiation). Finally, the PbSb $_2$ Te $_4$ ingots have rhombohedral symmetry with an inversely rotated axis $\overline{3}$. However, a hexagonal unit cell containing three rhombohedra is more convenient to study (Fig. 1). It has the following parameters: a = 0.4350 nm and c = 4.1712 nm. The PbSb $_2$ Te $_4$ compound has a 21-layer lattice and contains three seven-layer TeSbTePbTeSbTe packages, ordered in the direction of the hexagonal axis c (Shelimova et al. 2008), which is in good correlation with the results of numerical calculations of ideal crystals.

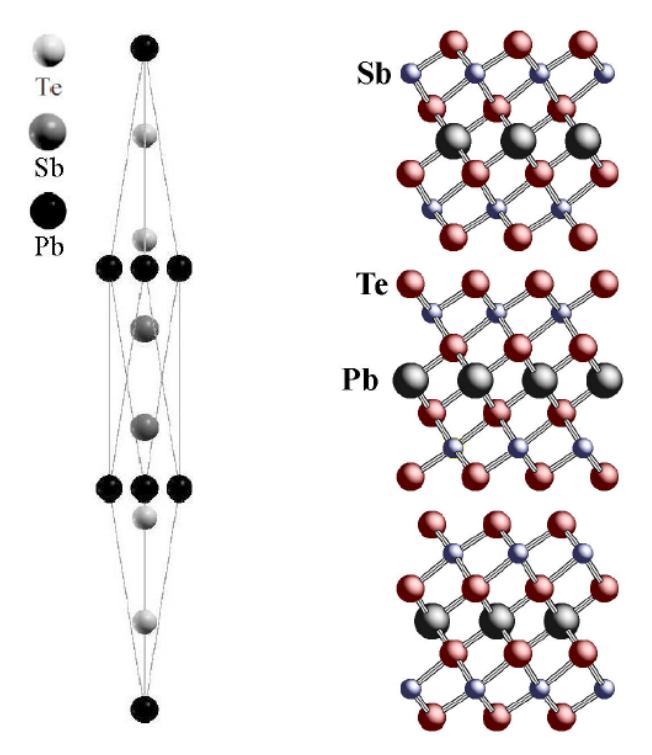


Fig. 1. The crystal structure of $PbSb_2Te_4$ in the form of a rhombohedral unit cell (left) and a hexagonal cell (right)

Further X-ray diffraction studies using a Bruker D8 Advance diffractometer in the Bragg–Brentano geometry (Cu-Ka radiation with a nickel filter) revealed the complex structure of the material and the existence of two phases: the basic PbSb₂Te₄ (70–80%) and Sb₂Te₃ (up to 20–30%) with rhombohedral symmetry, the spatial group R3m and the parameters of a hexagonal lattice about a = 0.426 nm, c = 3.045 nm. (Fig. 2). Also observed is the PbTe phase, mainly oriented perpendicular to the $\overline{3}$ axis, as well as traces of phases containing Sb and Te atoms.

Thus, the ingots are a periodic structure consisting of septuple and quintuple layers of $PbSb_2Te_4$ and Sb_2Te_2 compounds oriented along the trigonal axis $\overline{3}$.

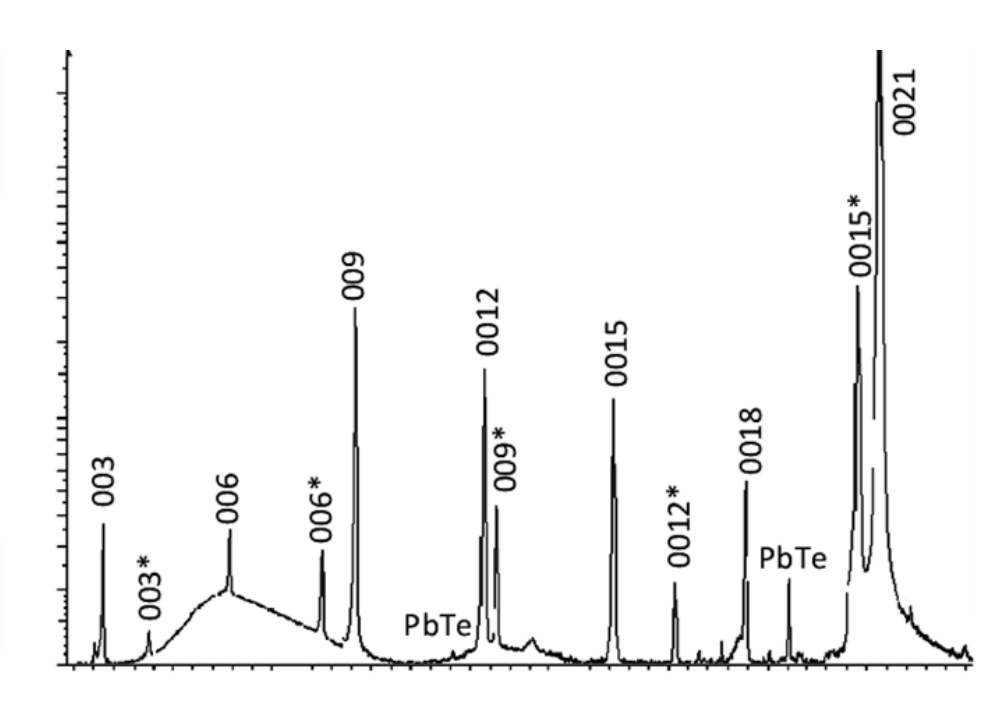


Fig. 2. Radiograph of the PbSb2Te4 ingot. Reflexes with the * sign and without * belong to the Sb_2Te_3 and $PbSb_2Te_4$ phases respectively

Two main phases have very similar values of the unit cell parameter a in the cleavage plane. Summarizing the experimental data and the data available in literature, we can note that despite the polyphasicity of the $PbSb_2Te_4$ ingots grown by the Chokhralsky method, they are characterized by a rhombohedral symmetry.

Information about the electronic spectrum of the studied samples and the structure of the valence band was obtained from the measurements of kinetic coefficients — electrical conductivity, Hall, Seebeck coefficients and the transverse Nernst–Ettingshausen effect — in two crystallographic directions: parallel and perpendicular to the hexagonal c axis. The kinetic coefficient tensors have a significant anisotropy corresponding to the rhombohedral symmetry of the ingots. Both components of the thermopower tensor are positive, so holes are the main current carriers. Their concentration was estimated from the Hall coefficient from the larger component, as is usually made for compounds $A_2^V B_3^{VT}$:

$$p \approx (eR)^{-1}$$
,

As already noted, tetradymite-like materials contain a large number of point defects. The process of the defect formation in $PbSb_2Te_4$ has been poorly studied, but it is clear that vacancy defects prevailing in chalcogenides are positive charged acceptor levels and create holes in the valence band. Measured low values of the components of the Hall tensor ($R_{123}\approx 0.02~cm^{-3}/K$) of $PbSb_2Te_4$ crystals indicate a high concentration of holes in these compounds. The material has a p-type conductivity and a hole concentration of $3.2\times 10^{20}~cm^{-3}$. In chalcogenide materials, vacancies in the metal sublattice in materials with hole conductivity play an important role, providing, respectively, the maximum concentration of current carriers in p-PbTe at the level of $1\times 10^{19}~cm^{-3}$ and in Sb_2Te_3 at the level of $1\times 10^{20}~cm^{-3}$ (Lu et al. 2012).

The values of four kinetic coefficients in cubic crystals are sufficient (Kaidanov et al. 1972) to determine the quadratic (parabolic) energy spectrum, including the effective mass of the density of states and the effective scattering cross section. A joint study of the temperature dependences of kinetic coefficients in the temperature range from 77 to 450 K makes an assessment of the efficiency of the mass density of states m^* and Fermi level ε_F at low temperature (T \approx 120K):

$$m^* = \left(\frac{3}{\pi}\right)^{2/3} \cdot \frac{\hbar^2}{T} \cdot p^{2/3} \cdot \frac{e}{k_0} \cdot \left(S - \frac{Q}{R\sigma}\right),$$

$$\varepsilon_F = \left(\frac{3p}{8\pi}\right)^{2/3} \cdot \frac{h^2}{2m^*},$$

where p — holes concentration, $\hbar = h/2\pi$ — Planck's constant, k_0 — Boltzmann's constant and e — the electron charge module. These formulas are valid for the quadratic law of variance in the case of quantum statistics.

The effective mass $m^* \approx 0.5 m_0$ (where m_0 is the mass of a free electron) and $\varepsilon_F \approx 0.15 eV$ at room temperature. At the same time, as temperatures increase, both components of electrical conductivity (in the cleavage plane and along the trigonal axis $\overline{3}$) decrease monotonically, i. e. show behavior characteristic of metals.

An essential feature of the carrier transfer phenomena is the observed increase in both Hall coefficients with temperature, which indicates the complex structure of the valence band and the involvement of holes with different effective masses in the transfer phenomena. In the two-band model, it is traditionally assumed that the growth of the Hall coefficients is associated with the pumping of holes from the main extremum to an additional one located near the Fermi level (Askerov 1994) (Fig. 3).

The calculated values of the charge carrier concentration in ${\rm PbSb_2Te_4}$ are not optimal for thermoelectric applications.

The addition of impurities to the initial mixture makes it possible to significantly modify the structure and properties of the resulting crystals. Given the high concentration of vacancy defects, it is interesting to study the samples of the compound PbSb₂Te₄, doped with a donor impurity, which is Cu.

We examined a series of Cu-doped samples as the formalism of the density functional theory using the pseudopotential method as well as the full-potential method of linearized coupled plane waves are rather limited in terms of calculating the defects of real crystals and the distribution of alloying impurities. The contribution of impurity atoms and defects in a real crystal can be considered by a change in the equilibrium carrier concentration.

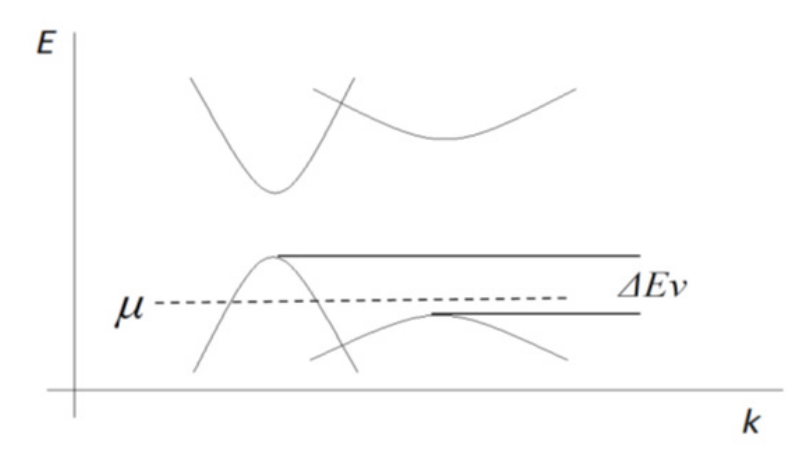


Fig. 3. $PbSb_2Te_4$ zone structure model. μ is the chemical potential, ΔEv is the energy gap between the unequal extremes of the valence band

The introduction of copper leads to a slight increase in the lattice parameter c. The obtained value of c = 4.1733 nm for the doped compound slightly exceeds the value of c = 4.1712 nm for the undoped PbSb₂Te₄. The addition of a copper impurity initially leads to an almost twofold increase in both components of the Hall tensor, which indicates a twofold decrease in the concentration of holes compared with an undoped crystal. However, a more significant decrease in the concentration of the main carriers was not achieved even with a twice increase in the proportion of the alloying additive in the initial mixture (PbTe+Sb₂Te₃)_{0.9995}Cu_{0.0005}. This effect can be explained if we assume the presence of several mechanisms for the incorporation of alloying additive atoms into the structure of the initial crystals. At the first stage, small amounts of copper atoms fill the vacancies. Filling such vacancies, in addition to reducing carrier concentration, should reduce phonon scattering and increase their mobility. With a further increase in the proportion of Cu atoms, these atoms presumably begin to settle in the interlayers between the septuple and quintuple layers, forming new copper-rich phases. Such inclusions should effectively scatter phonons along the hexagonal axis, reducing the lattice thermal conductivity.

When a donor copper impurity is introduced in a larger amount (PbTe+Sb $_2$ Te $_3$) $_{0.999}$ Cu $_{0.001}$ in addition to the main phases, the following components presumably could be identified in the samples: CuTe (ortho-rhombohedral lattice, a = 0.346 nm, c = 0.699 nm); Cu $_3$ Sb (ortho-rhombohedral lattice, a = 0.550 nm, c = 0.435 nm); Cu $_1$ Sb $_3$ (hexagonal lattice, a = 0.992 nm, c = 0.432 nm); Cu $_7$ Te $_4$ (hexagonal lattice, a = 0.832 nm, c = 0.726 nm) and Sb $_2$ Te (hexagonal lattice a = 0.418 nm, c = 1.747 nm).

To confirm the phase structure of the samples, additional measurements, such as Raman spectra, are needed and are currently underway.

According to the small size of Cu atoms ($R_{Cu} = 0.116$ nm) and the types of crystal lattices of the proposed minor phases, it can be assumed that, at least partially, these phases could be embedded in the Van der Waals gaps between the layers of the main phases.

The anisotropy of the Nernst–Ettingshausen coefficient observed when measuring the kinetic coefficients of the doped samples, viewed in a sign change during the transition from a component in which the carrier flow occurs exclusively in the cleavage plane to components in which the trajectory of the carrier flow intersects the cleavage plane, indicates a significant difference in the contributions of the dominant scattering mechanisms in different crystallographic directions. We can talk about the predominance of acoustic hole scattering in the cleavage plane and the significant influence of impurity scattering along the trigonal axis, which confirms the assumption of impurity localization between the septuple and quintuple layers of the main phases.

Conclusions

Our study of a series of samples of PbSb₂Te₄ crystals grown by the Chokhralsky method discovered that ingots are periodic structures oriented along a trigonal axis which are multiphase with dominant phases PbSb₂Te₄ and Sb₂Te₅.

The experiments on the doping of PbSb₂Te₄ crystals have shown that small amounts of Cu atoms are likely to occupy vacancies in the metal sublattice. As the amount of copper in the initial mixture increases, impurity atoms presumably enter into a chemical bond with Sb and Te atoms.

The charge transfer phenomena were also investigated. Based on the measurements of four kinetic coefficients in the temperature range of $77-450~\rm K$, the parameters of the band spectrum of current carriers were estimated. The growth of the Hall coefficient indicates the involvement of several types of holes in the transfer phenomena.

Conflict of Interest

The authors declare that there is no conflict of interest, either existing or potential.

Author Contributions

S. A. Nemov designed and directed the project; V. D. Andreeva performed the measurements and analysed the spectra, A. Yu. Aliabev processed the experimental data, performed the analysis, drafted the manuscript and designed the figures. All the authors discussed the final work and took part in writing the article.

References

- Aguilera, I., Friedrich, C., Bihlmayer, G. et al. (2013) GW study of topological insulators Bi2Se3, Bi2Te3, and Sb2Te3: Beyond the perturbative one-shot approach. *Physical Review B*, 88 (4), article 045206. https://doi.org/10.1103/PHYSREVB.88.045206 (In English)
- Askerov, B. M. (1994) *Electron Transport Phenomena in Semiconductors*. Singapore: World Scientific Publ., 394 p. (In English)
- Chen, Y. L., Analytis, J. G., Chu, J.-H. et al. (2009) Experimental realization of a three-dimensional topological insulator Bi2Te3. *Science*, 325, 178–181. https://doi.org/10.1126/science.1173034 (In English)
- Hattori, Y., Sagisaka, K., Yoshizawa, S. et al. (2023) Topological surface states hybridized with bulk states of Bi-doped PbSb2Te4 revealed in quasiparticle interference. *Physical Review B*, 108 (12), article 121408. https://doi.org/10.1103/physrevb.108.1121408 (In English)
- Jayan, K. D., Rakesh, P. (2022) First principles roadmap to topological insulators for quantum computing applications. *Recent Trends in Chemical and Material Sciences*, 8, 136–148. https://doi.org/10.9734/bpi/rtcams-v8/2319B (In English)
- Kaidanov, V. I., Erasova, N. A., Zhitinskaya, M. K. (1972) Kineticheskie yavleniya v poluprovodnikakh [Kinetic phenomena in semiconductors]. Leningrad: Kalinin Leningrad Polytechnic Institute Publ., 79 p. (In Russian)
- Lu, P., Wang, X., Lu, M. (2012) Largely enhanced thermoelectric properties of the binary-phased PbTe–Sb2Te3 nanocomposites. *Journal of Materials Research*, 27, 734–739. https://doi.org/10.1557/jmr.2011.44110 (In English)
- Menshchikova, T. V., Eremeev, S. V., Chulkov, E. V. (2013) Electronic structure of SnSb2Te4 and PbSb2Te4 topological insulators. *Applied Surface Science*, 267, 1–3. https://doi.org/10.1016/J.APSUSC.2012.04.048 (In English)
- Shelimova, L. E., Karpinski, O. G., Konstantinov, P. P. et al. (2008) Anizotropnye termoelektricheskie materialy dlya termogeneratorov na osnove sloistykh tetrademitopodobnykh khal'kogenidov [Anisotropic thermoelectric materials for thermogenerators based on layered tetradimite-like chalcogenides]. *Perspektivnye materialy*, 2, 28–38. (In Russian)
- Shelimova, L. E., Karpinskii, O. G., Svechnikova, T. E. et al. (2004) Synthesis and structure of layered compounds in the PbTe-Bi2Te3 and PbTe-Sb2Te3 systems. *Inorganic Materials*, 40 (5), 1264–1270. https://doi.org/10.1007/s10789-005-0069-1 (In English)
- Wang, K. L., Lang, M., Kou, X. (2016) Spintronics of Topological Insulators. In: Y. Xu, D. Awschalom, J. Nitta (eds.). *Handbook of Spintronics*. Dordrecht: Springer Publ., pp. 431–462. https://doi.org/10.1007/978-94-007-6892-5-56 (In English)



Theoretical physics.
Physics of atoms and molecules

UDC 539.1

EDN WTKYUL

https://www.doi.org/10.33910/2687-153X-2025-6-3-150-154

Pseudopotential method for coupling matrix element calculations

S. A. Yakovleva ^{□1}, V. A. Vahrushev ¹, I. G. Stepanov ², A. K. Belyaev ¹

¹ Herzen State Pedagogical University of Russia, 48 Moika Emb., Saint Petersburg 191186, Russia ² ITMO University, 49 Kronverksky Pr., Saint Petersburg 197101, Russia

Authors

Svetlana A. Yakovleva, ORCID: <u>0000-0002-8889-7283</u>, e-mail: <u>sayakovleva@herzen.spb.ru</u>

Vsevolod A. Vahrushev, ORCID: <u>0000-0002-6821-4529</u>

Ilya G. Stepanov, ORCID: 0009-0008-4476-2548

Andrey K. Belyaev, ORCID: 0000-0001-8834-1456, e-mail: belyaev@herzen.spb.ru

For citation: Yakovleva, S. A., Vahrushev, V. A., Stepanov, I. G., Belyaev, A. K. (2025) Pseudopotential method for coupling matrix elements calculations. *Physics of Complex Systems*, 6 (3), 150–154. https://www.doi.org/10.33910/2687-153X-2025-6-3-150-154 EDN WTKYUL

Received 20 May 2025; reviewed 27 June 2025; accepted 1 July 2025.

Funding: the research was supported by an internal grant of Herzen State Pedagogical University of Russia (project No. 46-VG).

Copyright: © S. A. Yakovleva, V. A. Vahrushev, I. G. Stepanov, A. K. Belyaev (2025). Published by Herzen State Pedagogical University of Russia. Open access under <u>CC BY License 4.0</u>.

Abstract. This work derives electronic Hamiltonian matrix elements in diabatic representation using an asymptotic approach. Off-diagonal matrix elements which couple different covalent excited states of a LiH quasi-molecule with an ionic molecular state are calculated. Electronic wave functions of different lithium states are determined by both the Discrete Variable Representation (DVR) and pseudopotential methods. Electronic wave functions of a hydrogen negative ion are obtained by the complex rotation method.

Keywords: inelastic processes, nonadiabatic transitions, pseudopotential, electronic Hamiltonian, hydrogen negative ion

Introduction

There is a wide variety of methods for calculating the electronic structure of a quasi-molecule. Both adiabatic and diabatic representations can be used. In adiabatic representation, eigenfunctions of the electronic Hamiltonian ψ_j^{ad} are used to determine the eigenvalues of the electronic Hamiltonian $\langle \psi_j^{ad} | \hat{H}_j | \psi_k^{ad} \rangle$ as well as non-adiabatic coupling matrix elements $\langle \psi_j^{ad} | \frac{\partial}{\partial R} | \psi_k^{ad} \rangle$, $\langle \psi_j^{ad} | L_x^2 + L_y^2 | \psi_k^{ad} \rangle$ and so on. In diabatic representation, the basis of diabatic functions ψ_j^{di} is used to determine the diagonal and off-diagonal matrix elements of the electronic Hamiltonian $\langle \psi_j^{di} | \hat{H}_j | \psi_k^{di} \rangle$. The aforementioned quantities are used in the studies of nuclear dynamics of colliding systems in terms of the Born–Oppenheimer approach. The choice of electronic basis functions (adiabatic or diabatic) defines the system of coupled channel differential equations for nuclear wave functions.

This paper proposes a method based on the asymptotic approach for calculating the electronic Hamiltonian matrix elements in diabatic representation for collisions of atoms and positive ions of different chemical elements with atoms and negative ions of hydrogen. The main focus of this work is calculating the off-diagonal matrix element of the electronic Hamiltonian that corresponds to the interaction

of ionic and covalent configurations. Molecular wave functions of the covalent states are constructed using the one-electron wave functions computed on Discrete Variable Representation (DVR) basis functions with the pseudopotential method. Hydrogen negative ion wave function calculated using the complex rotation method (Yarevsky 2016) is used as the ionic state wave function.

Theory

The asymptotic approach was proposed for studying inelastic processes in (Belyaev 2013). The electron structure of a quasimolecule formed in collisions of atoms and ions of various elements with atoms and ions of hydrogen is modeled by constructing the electronic Hamiltonian matrix in diabatic representation. An important step is the calculation of the off-diagonal matrix elements which define interactions between different states of the quasimolecule. In terms of the asymptotic approach, only the ion-covalent couplings are taken into account, and for determining the off-diagonal matrix elements charge exchange formula (Olson et al. 1971) is used. This paper proposes calculating the matrix elements of ion-covalent interaction by use of asymptotic expressions for covalent state wave functions of the quasimolecule and negative hydrogen ion wave function calculated using the complex rotation method.

To model the electronic structure of a LiH quasimolecule using the asymptotic approach, we consider several covalent states $Li(1s^2nl^2L) + H(1s^2S)$ and one ionic state $Li^+(1s^2 S) + H^-(1s^2 S)$, including only ${}^1\Sigma^+$ molecular states. The electronic hamiltonian for this system reads

$$\begin{split} \widehat{H}_{e} &= -\frac{\hbar^{2}}{2m_{e}} \Delta_{\vec{r}_{1}} - \frac{\hbar^{2}}{2m_{e}} \Delta_{\vec{r}_{2}} - \frac{Ze^{2}}{4\pi\varepsilon_{0}r_{1H}} - \frac{Ze^{2}}{4\pi\varepsilon_{0}r_{1Li}} - \\ &- \frac{Ze^{2}}{4\pi\varepsilon_{0}r_{2H}} - \frac{Ze^{2}}{4\pi\varepsilon_{0}r_{2Li}} + \frac{Ze^{2}}{4\pi\varepsilon_{0}R} + \frac{Ze^{2}}{4\pi\varepsilon_{0}r_{12}}, \end{split} \tag{1}$$

where electron coordinates $\vec{r_1}$ and $\vec{r_2}$ are measured from the center of the nuclear mass, R is internuclear distance, r_{1H} , r_{2H} , r_{1Li} , r_{2Li} are the distances from the first or second electron to the hydrogen or lithium core, and r_{12} is the distance between two electrons.

The asymptotic molecular wave function $|L\tilde{\Lambda}SM_S\rangle$ for covalent ${}^1\Sigma^+$ ($\tilde{\Lambda}=0$, S = 0, $M_S=0$) molecular states of LiH is constructed using one-electron atomic wave functions using the expression from (Nikitin, Umanskii 1984) and reads:

$$|L000\rangle = \hat{A} \sum_{m_{s1}, m_{s2}} C_{\frac{1}{2}m_{s1}\frac{1}{2}m_{s2}}^{0} \varphi_{nl0}^{Li}(\vec{r}) \chi_{\frac{1}{2}m_{s1}}(\sigma) \cdot \varphi_{100}^{H}(\vec{r}') \chi_{\frac{1}{2}m_{s2}}(\sigma'), \tag{2}$$

where \hat{A} is an antisymmetrization operator, $C^{JM}_{j_1\,m_1\,j_2\,m_2}$ denotes Clebsch–Gordan coefficients, and $\varphi^{\alpha}_{nlm}(\vec{r})Xsm_s(\sigma)$ is the wave function of an electron centered on the hydrogen or lithium core (α being H or Li). The antisymmetric wave function if the ionic state is expressed as follows:

$$|0000\rangle = \frac{1}{\sqrt{2}}\psi_{H^{-}}(r_{1H}, r_{2H}, \cos\theta_{12}) \left(\chi_{\frac{1}{2}\frac{1}{2}}(\sigma_{1})\chi_{\frac{1}{2}-\frac{1}{2}}(\sigma_{2}) - \chi_{\frac{1}{2}-\frac{1}{2}}(\sigma_{1})\chi_{\frac{1}{2}\frac{1}{2}}(\sigma_{2})\right), \tag{3}$$

where $\Psi_{H} - (r_{1H}, r_{2H}, cos\theta_{12})$ is the wave function of two electrons in the negative hydrogen ion, θ_{12} being the angle between \vec{r}_{1H} and \vec{r}_{2H} .

Using these molecular wave functions, the off-diagonal matrix element of the electronic Hamiltonian (1) can be expressed via coordinate one-electron atomic functions and the function of the hydrogen negative ion:

$$\langle L000 | \hat{H}_{e} | 0000 \rangle = \frac{1}{2\sqrt{2(1+s^{2})}} \left[2 \left(E_{H^{-}} + \frac{Ze^{2}}{4\pi\varepsilon_{0}R} \right) S - \frac{e^{2}}{4\pi\varepsilon_{0}} \left(\left\langle \varphi_{100}(\vec{r}_{2H})\varphi_{nl0}(\vec{r}_{1Li}) \right| \frac{1}{r_{1Li}} + \frac{1}{r_{2Li}} \left| \psi_{H^{-}}(r_{1H}, r_{2H}, \cos\theta_{12}) \right\rangle + \left\langle \varphi_{100}(\vec{r}_{1H})\varphi_{nl0}(\vec{r}_{2Li}) \right| \frac{1}{r_{1Li}} + \frac{1}{r_{2Li}} \left| \psi_{H^{-}}(r_{1H}, r_{2H}, \cos\theta_{12}) \right\rangle \right) \right]$$

$$(4)$$

where s and S are overlap integrals:

$$s = \langle \varphi_{nl0}(\vec{r}_{1Li}) | \varphi_{100}(\vec{r}_{2H}) \rangle = \langle \varphi_{nl0}(\vec{r}_{2Li}) | \varphi_{100}(\vec{r}_{1H}) \rangle,$$

$$S = \langle \varphi_{100}(\vec{r}_{2H}) \varphi_{nl0}(\vec{r}_{1Li}) | \psi_{H^{-}}(r_{1H}, r_{2H}, \cos \Theta_{12}) \rangle =$$

$$\langle \varphi_{100}(\vec{r}_{1H}) \varphi_{nl0}(\vec{r}_{2Li}) | \psi_{H^{-}}(r_{1H}, r_{2H}, \cos \Theta_{12}) \rangle.$$

To find the actual values of the off-diagonal matrix element (4), one needs to calculate several similar 6-dimensional integrals. In the present work we perform integration over the coordinates of two electrons, measured from the hydrogen core as follows:

$$\langle \varphi_{100}(\vec{r}_{2H})\varphi_{nl0}(\vec{r}_{1Li})|\frac{1}{r_{1Li}}|\psi_{H^{-}}(r_{1H},r_{2H},\cos\theta_{12})\rangle =$$

$$= \int_{0}^{\pi} \int_{0}^{2\pi} \int_{0}^{\infty} \int_{0}^{\pi} \int_{0}^{2\pi} \int_{0}^{\infty} \frac{\varphi_{100}(\vec{r}_{2H})\varphi_{nl0}(\vec{r}_{1Li})\psi_{H^{-}}(r_{1H},r_{2H},\cos\theta_{12})}{r_{1Li}} \cdot r_{1H}^{2} \sin\theta_{1H} dr_{1H} d\theta_{1H} d\varphi_{1H} r_{2H}^{2} \sin\theta_{2H} dr_{2H} d\theta_{2H} d\varphi_{2H}$$
(5)

In order to use the wave function of the hydrogen negative ion, we define $cos\theta_{12}$ from the scalar product of \vec{r}_{1H} and \vec{r}_{2H} ; the distance r_{1L} is defined via r_{1H} and r_{2H} .

These equations make it possible to calculate the off-diagonal matrix element of the electronic Hamiltonian in diabatic representation for a particular internuclear distance R. In order to study non-adiabatic nuclear dynamics — for example, using the multichannel Landau—Zener model — one needs to know both diagonal and off-diagonal matrix elements for a range of internuclear distances.

Results

In this work we consider the following excited states of Li(2s, 2p, 3s, 3p, 4s, 4p) for molecular wave functions of the covalent states $\text{Li}(1\text{s}^2\text{nl}\ ^2\text{L}) + \text{H}(1\text{s}\ ^2\text{S})$ defined by Eq. (2). The wave function of one electron centered on the lithium core is calculated by expanding it over the basis of DVR functions with the use of a pseudopotential. The dependence of the pseudopotential on r is calculated using the tabulated wave function of a 2s-electron in a Li atom from (Clementi, Roetti 1974). The wave function of two electrons in the hydrogen negative ion is calculated by the complex rotation method (Yarevsky 2016).

Fig. 1 shows the probability density of two electrons as a function of two distances from the nucleus to both electrons ($\vec{r_1}$ and $\vec{r_2}$) for a fixed angle between these radius vectors. The upper panel depicts the case of equal distances ($r_1 = r_2$) for two geometries of the particles: the angle between electron radius vectors equals 0 and π . The electron correlation is clearly seen. The lower panel demonstrates the dependence of the electronic probability density on the distance from the nucleus to one electron while the distance to another electron is fixed. We can see that the maximum of the density corresponds to the case when both electrons are close to the nucleus (both distances are around 1–3 a. u.) and the two-electron wave function can be represented as a product of two equivalent single-electronic wave functions. When one of the electrons moves away, the electronic configuration changes and the two-electronic wave function becomes a product of two non-equivalent single-electronic wave functions.

Finally, the off-diagonal matrix elements of the electronic Hamiltonian are calculated using Eq. (4). The comparison of the calculated data with the values from quantum chemical calculations (Croft et al. 1999) and given by a semi-empirical formula for one electron charge transfer (Olson et al. 1971) is presented in Fig. 2.

The graphs demonstrate the general agreement of the off-diagonal Hamiltonian matrix elements calculated in the present work with the results of the previous calculations for a LiH molecule (Croft et al. 1999) as well as the semi-empirical estimates (Olson et al. 1971). These dependences have the exponential form that agrees with the asymptotic theory. The difference of the data calculated in the present work from the results of quantum chemical calculations can be related to the fact that the pseudopotential is obtained using the wave function of the 2s-electron. It is worth noting that for calculations of the wave functions for higher excited states of the Li atom, the larger basis of DVR functions should be used, which can also lead to deviations of the obtained results from the quantum chemical data.

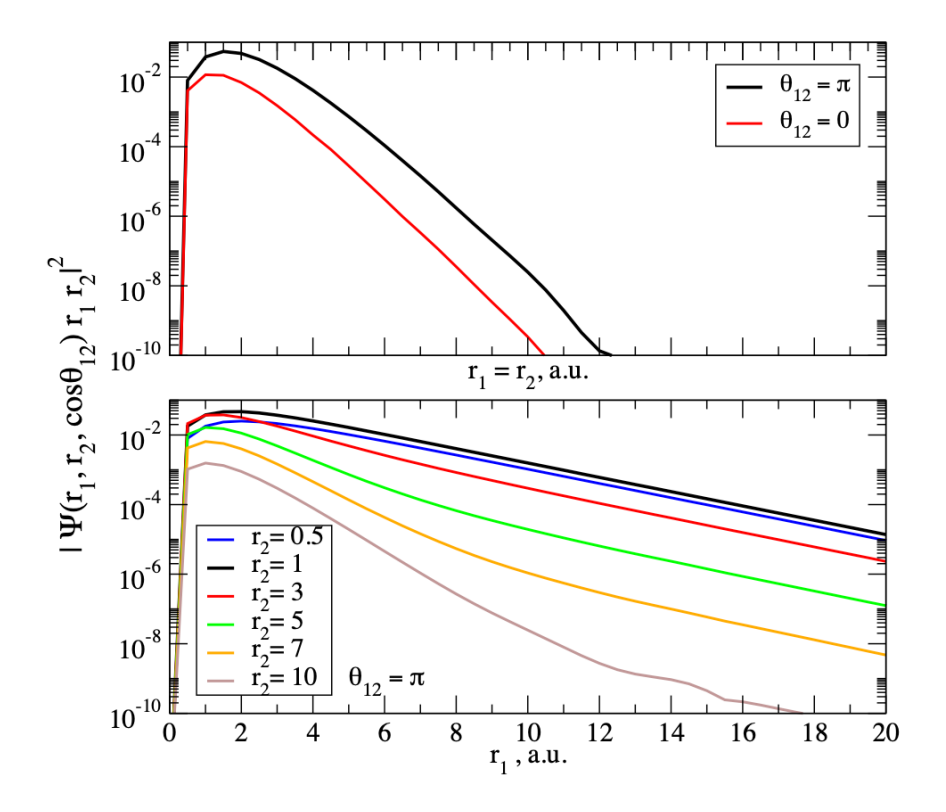


Fig. 1. The probability density of two electrons in a negative hydrogen ion calculated by the complex rotation method

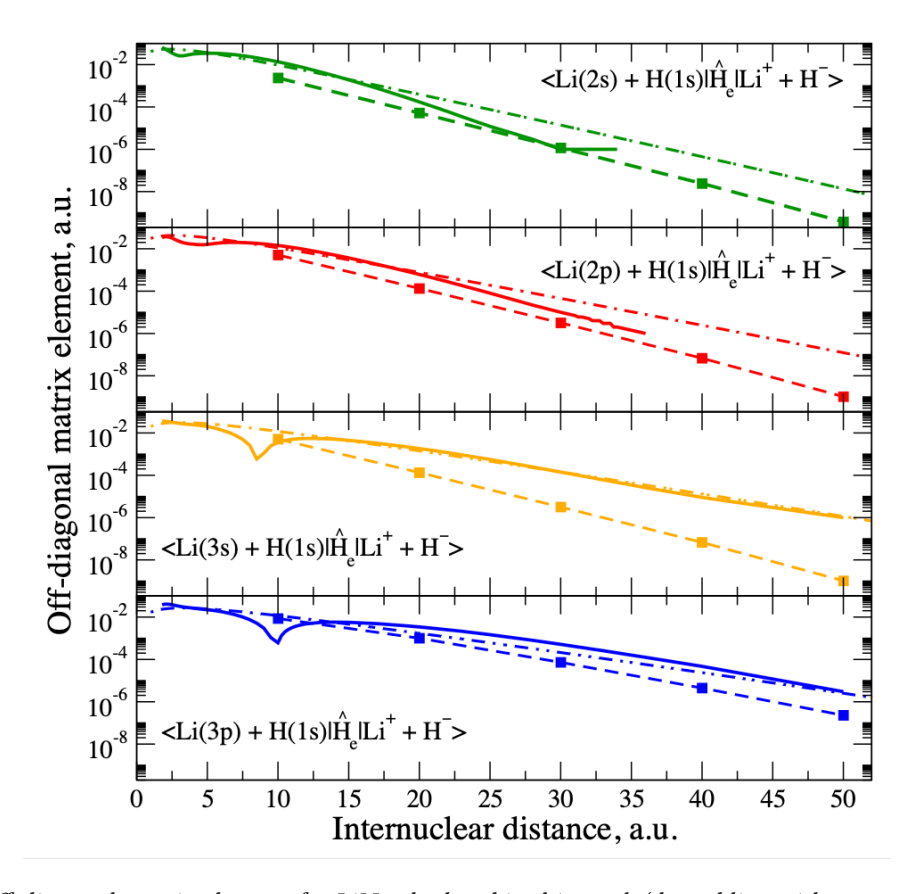


Fig. 2. The off-diagonal matrix element for LiH calculated in this work (dotted line with squares), by a semiempirical formula (dash-dotted line) and in quantum chemical calculations (solid line) for 2s (upper panel), 2p (second from the top panel), 3s (second from the bottom panel), and 3p (bottom panel) electron in a Li atom

Conclusion

The off-diagonal electronic Hamiltonian matrix elements are calculated using the accurate wave function of the two electrons in the hydrogen negative ion and the wave functions of the six excited states of the lithium atom, calculated by means of the DVR basis functions and the pseudopotential taken from the accurate ab initio Hartree–Fock calculations. The calculated matrix elements can be used for accurate nuclear dynamics studies determining the non-adiabatic transition probabilities and inelastic cross sections in the lithium-hydrogen collisions, by means of the wave packet method (Yakovlev, Belyaev 2024), the reprojection method (Belyaev 2022), and probability currents method (Stepanov, Belyaev 2024).

Conflict of Interest

The authors declare that there is no conflict of interest, either existing or potential.

Author Contributions

Each of the authors has contributed to the submission.

Acknowledgements

The authors gratefully acknowledge the assistance with obtaining the wave function of the hydrogen negative ion provided by Dr. E. Yarevsky in private communication.

References

- Belyaev, A. K. (2013) Model approach for low-energy inelastic atomic collisions and application to Al + H and Al⁺ + H⁻. *Physical Review A*, 88 (5), article 052704. https://doi.org/10.1103/PhysRevA.88.052704 (In English)
- Belyaev, A. K. (2022) Reprojection method for inelastic processes in atomic collisions within Born-Oppenheimer approach. *Physics of Complex Systems*, 3 (1), 25–36. https://doi.org/10.33910/2687-153X-2022-3-1-25-36 (In English)
- Clementi, E., Roetti, C. (1974) Roothan-Hartree-Fock atomic wavefunctions: Basis functions and their coefficients for ground and certain excited states of neutral and ionized atoms, Z≤54. *Atomic Data and Nuclear Data Tables*, 14 (3–4), 177–478. https://doi.org/10.1016/S0092-640X(74)80016-1 (In English)
- Croft, H., Dickinson, A. S., Gadea, F. X. (1999) A theoretical study of mutual neutralization in Li⁺ + H⁻ collisions. *Journal of Physics B: Atomic, Molecular and Optical Physics*, 32 (1), article 81. https://doi.org/10.1088/0953-4075/32/1/008 (In English)
- Nikitin, E. E., Umanskii, S. Y. (1984) *Theory of Slow Atomic Collisions*. Berlin: Springer Publ., 434 p. (In English) Olson, R. E., Smith, F. T., Bauer, E. (1971). Estimation of the coupling matrix elements for one-electron transfer systems. *Applied Optics*, 10 (8), 1848–1855. https://doi.org/10.1364/AO.10.001848 (In English)
- Stepanov, I. G., Belyaev, A. K. (2024) Probability currents in inelastic atomic collision studies. *Physics of Complex Systems*, 5 (2), 74–82. https://doi.org/10.33910/2687-153X-2024-5-2-74-82 (In English)
- Yakovlev, M. Yu., Belyaev, A. K. (2024) The hyperbolic matrix method for wave packet treatment of atomic and molecular dynamics. *Physics of Complex Systems*, 5 (1), 21–29. https://doi.org/10.33910/2687-153X-2024-5-1-21-29 (In English)
- Yarevsky, E. (2016) Scattering problem and resonances for three-body Coulomb quantum systems: parallel calculations. *EPJ Web of Conferences*, 108, article 02046. https://doi.org/10.1051/epjconf/201610802046 (In English)

Summaries in Russian / Информация о статьях на русском языке

Физика конденсированного состояния

ВЛИЯНИЕ ПОПЕРЕЧНОГО ЭЛЕКТРИЧЕСКОГО ПОЛЯ НА СОПРОТИВЛЕНИЕ ТОНКИХ ПЛЕНОК ВІ НА ПОДЛОЖКЕ ИЗ СЛЮДЫ И ПОЛИАМИДА

Владимир Алексеевич Комаров, Владимир Минович Грабов, Вероника Витальевна Простова Аннотация. Работа посвящена исследованию влияния поперечного электрического поля на сопротивление тонких пленок висмута. В работе экспериментально подтверждено существование эффекта электрического поля в тонких пленках висмута на слюде и полиамиде. Получены экспериментальные зависимости сопротивления от напряженности поперечного электрического поля для пленок висмута различной толщины на слюде и полиамиде. Выявлены изменения, происходящие при уменьшении толщины пленки и материала использованной подложки. Дана качественная интерпретация наблюдаемого эффекта на основе анализа изменения подвижности свободных носителей заряда в пленках в зависимости от направления электрического поля, а также толщины пленки и материала подложки.

Ключевые слова: висмут, тонкие пленки, сопротивление, эффект поперечного электрического поля

Для цитирования: Komarov, V. A., Grabov, V. M., Prostova, V. V. (2025) Effect of a transverse electric field on the resistance of Bi thin films on a mica and polyimide substrate. *Physics of Complex Systems*, 6 (3), 121–126. https://www.doi.org/10.33910/2687-153X-2025-6-3-121-126 EDN AJAUNX

ОСОБЕННОСТИ МИКРОСТРУКТУРЫ СФЕРОЛИТОВЫХ ТОНКИХ ПЛЕНОК ЦИРКОНАТА ТИТАНАТА СВИНЦА

Владимир Петрович Пронин, Артемий Николаевич Крушельницкий, Михаил Владимирович Старицын, Станислав Викторович Сенкевич, Евгений Юрьевич Каптелов, Игорь Петрович Пронин, Владислав Андреевич Томковид

Аннотация. Методами растровой электронной микроскопии исследовались отличия микроструктуры сферолитовых пленок ЦТС, в которой реализуется малоугловое некристаллическое и кристаллическое ветвление в процессе кристаллизации фазы перовскита. Предполагается, что наблюдаемые в пленках циркулярно-ступенчатые и радиальные границы формируются за счет механизма дисклинации, в то время как их отсутствие является результатом последовательного образования одиночных краевых дислокаций.

Ключевые слова: сферолиты, тонкие пленки ЦТС, механические напряжения, механизмы поворота кристаллической решетки

Для цитирования: Pronin, V. P., Krushelnitckii, A. N., Staritsyn, M. V., Senkevich, S. V., Kaptelov, E. Yu., Pronin, I. P., Tomkovid, V. A. (2025) Microstructure features of spherulitic lead zirconate titanate thin films. *Physics of Complex Systems*, 6 (3), 127–133. https://www.doi.org/10.33910/2687-153X-2025-6-3-127-133 EDN ESOLRP

Физика полупроводников

СПЕКТРЫ И КИНЕТИКА СЕНСИБИЛИЗИРОВАННОГО КРАСИТЕЛЕМ ФОТОВОЛЬТАИЧЕСКОГО ЭФФЕКТА В КРЕМНИИ

Михаил Александрович Горяев, Александр Павлович Смирнов

Аннотация. Исследовано влияние находящихся на поверхности полупроводников молекул органического красителя на проявление фотовольтаического эффекта в образцах кремния с различными типами проводимости. Наблюдается спектральная сенсибилизация фото-ЭДС в полосе поглощения красителя для монокристаллических образцов с проводимостью *п*-типа и десенсибилизация в образцах с проводимостью *р*-типа. Также имеются существенные различия

в кинетике фотовольтаического эффекта в области поглощения красителя в полупроводниках с различным типом проводимости: в кремнии n-типа наблюдается монотонный рост фото-ЭДС, а в кремнии p-типа фото-ЭДС сначала растет, а затем происходит ее падение. В порошкообразных образцах наблюдается эффективная сенсибилизация фотопроводимости на постоянном токе как для полупроводников p-типа. Обсуждается различный вклад генерированных при безызлучательном индуктивно-резонансном переносе энергии от красителя полупроводнику электронов и дырок в разные виды фотоэффекта.

Ключевые слова: кремний с различным типом проводимости, кремний с адсорбированным красителем, спектральная сенсибилизация, фото-ЭДС, фотопроводимость на постоянном токе, сенсибилизация фотовольтаического эффекта красителями

Для цитирования: Goryaev, M. A., Smirnov, A. P. (2025) Spectra and kinetics of dye-sensitized photovoltaic effect in silicon. *Physics of Complex Systems*, 6 (3), 134–138. https://www.doi.org/10.33910/2687-153X-2025-6-3-134-138 EDN GAMNFT

АНАЛИЗ ЛОКАЛЬНОЙ СТРУКТУРЫ БЛИЖНЕГО ОКРУЖЕНИЯ АТОМОВ ГЕРМАНИЯ В ХАЛЬКОГЕНИДНЫХ СПЛАВАХ $\mathrm{GE_2SB_2TE_5}$ С ПОМОЩЬЮ МЕТОДА МЁССБАУЭРОВСКОЙ СПЕКТРОСКОПИИ

Алла Валентиновна Марченко, Юрий Александрович Петрушин, Павел Павлович Серегин, Вячеслав Александрович Доронин

Аннотация. Методом мессбауэровской спектроскопии на изотопе 73 Ge продемонстрирована тетраэдрическая симметрия локального окружения атомов германия в аморфных пленках $Ge_2Sb_2Te_5$. Сделан вывод о существенной разнице в ближайшем окружении и, следовательно, в электронных структурах атомов Ge в кристаллических и аморфных пленках $Ge_2Sb_2Te_5$. Рентгеноаморфные пленки $Ge_2Sb_2Te_5$ толщиной $20~\mu m$ были получены методом магнетронного распыления синтезированных поликристаллических образцов на постоянном токе в атмосфере азота на подложки из алюминиевой фольги. Затем пленки отжигали в интервале температур $150-200^{\circ}C$ для получения поликристаллических образцов. Состав пленок контролировался методом рентгенофлуоресцентного анализа.

Ключевые слова: мессбауэровская спектроскопия, $Ge_2Sb_2Te_5$, локальное окружение Ge, магнетронное распыление, рентгенофлуоресцентный анализ

Для цитирования: Marchenko, A. V., Petrushin, Yu. A., Seregin, P. P., Doronin, V. A. (2025) Analysis of the local structure of the nearest environment of germanium atoms in chalcogenide alloys $Ge_2Sb_2Te_5$ using the Mössbauer spectroscopy method. *Physics of Complex Systems*, 6 (3), 139–143. https://www.doi.org/10.33910/2687-153X-2025-6-3-139-143 EDN <u>SANBNC</u>

СОСТАВ, СТРУКТУРА И ОСОБЕННОСТИ СВОЙСТВ КРИСТАЛЛОВ РЬSb $_2$ Te $_4$, ВЫРАЩЕННЫХ МЕТОДОМ ЧОХРАЛЬСКОГО

Сергей Александрович Немов, Валентина Дмитриевна Андреева, Алексей Юрьевич Алябьев **Аннотация.** В данной работе приведены и проанализированы результаты рентгеноструктурных и физических исследований кристаллов $PbSb_2Te_4$, выращенных методом Чохральского. На качественном и количественном уровне обсуждаются особенности фазового состава и кристаллической структуры слитков, в том числе легированных донорной примесью меди. Образцы представляют собой периодическую структуру, являются многофазными, доминирующие фазы $PbSb_2Te_4$ и Sb_2Te_3 . Наличие собственных точечных электрически активных дефектов обуславливает высокую концентрацию дырок р $\approx 3.2 \times 10^{20}$ см $^{-3}$. Температурные зависимости кинетических коэффициентов свидетельствуют в пользу сложного строения валентной зоны. Атомы примеси при легировании занимают вакансии в металлической подрешетке и образуют химические соединения с атомами Sb и Te.

Ключевые слова: полупроводник, $PbSb_{2}Te_{4}$, термоэлектричество, топологический изолятор, тетрадимиты, легирование, кинетические коэффициенты, нанокомпозиты, рентгеноструктурный анализ, температурные зависимости коэффициента Холла, структура валентной зоны

Для цитирования: Nemov, S. A., Andreeva, V. D., Aliabev, A. Yu. (2025) Composition, structure and properties of PbSb $_2$ Te $_4$ crystals grown by the Chokhralsky method. *Physics of Complex Systems*, 6 (3), 144–149. https://www.doi.org/10.33910/2687-153X-2025-6-3-144-149 EDN RBTYMA

Теоретическая физика

ПРИМЕНЕНИЕ МЕТОДА ПСЕВДОПОТЕНЦИАЛА ДЛЯ РАСЧЕТОВ МАТРИЧНЫХ ЭЛЕМЕНТОВ НЕАДИАБАТИЧЕСКОЙ СВЯЗИ

Светлана Анатольевна Яковлева, Всеволод Алексеевич Вахрушев, Илья Григорьевич Степанов, Андрей Константинович Беляев

Аннотация. В работе приведены выражения для расчетов матричных элементов электронного гамильтониана в диабатическом представлении в рамках асимптотического подхода. Проведены расчеты недиагональных матричных элементов, связывающих различные возбужденные ковалентные состояния квазимолекулы LiH с ионным молекулярным состоянием. Для определения функций электрона в различных состояниях лития используются функции дискретного представления переменной и метод псевдопотенциала, а для волновой функции отрицательного иона водорода использованы результаты применения метода комплексных вращений.

Ключевые слова: неупругие процессы, неадиабатические переходы, псевдопотенциал, электронный потенциал, отрицательный ион водорода

Для цитирования: Yakovleva, S. A., Vahrushev, V. A., Stepanov, I. G., Belyaev, A. K. (2025) Pseudopotential method for coupling matrix elements calculations. *Physics of Complex Systems*, 6 (3), 150–154. https://www.doi.org/10.33910/2687-153X-2025-6-3-150-154 EDN <u>WTKYUL</u>